J|A|C|S
ARTICLES
Published on Web 06/07/2006

Nonchelated Alkene and Alkyne Complexes of d^0 Zirconocene Pentafluorophenyl Cations

Edward J. Stoebenau, III and Richard F. Jordan*

Contribution from the Department of Chemistry, The University of Chicago, 5735 South Ellis Avenue, Chicago, Illinois 60637

Received November 3, 2005; Revised Manuscript Received April 26, 2006; E-mail: rfjordan@uchicago.edu

Abstract: This paper describes the generation and properties of nonchelated d^0 zirconocene−aryl−alkene and alkyne adducts that are stabilized by the presence of β-$SiMe_3$ substituents on the substrates and the weak nucleophilicity of the $-C_6F_5$ ligand. The cationic complexes $[(C_5H_4R)_2Zr(C_6F_5)][B(C_6F_5)_4]$ (**4a**: R = H, **4b**: R = Me) were generated by methide abstraction from $(C_5H_4R)_2Zr(C_6F_5)Me$ by Ph_3C^+. NMR studies show that **4a**,**b** contain an *o*-CF···Zr dative interaction and probably coordinate a PhCl molecule in PhCl solution. Addition of allyltrimethylsilane (ATMS) to **4a**,**b** in C_6D_5Cl solution at low temperature produces an equilibrium mixture of $(C_5H_4R)_2Zr(C_6F_5)(H_2C{=}CHCH_2SiMe_3)^+$ (**7a**,**b**), **4a**,**b**, and free ATMS. Similarly, addition of propargyltrimethylsilane (PTMS) to **4a** produces an equilibrium mixture of $Cp_2Zr(C_6F_5)(HC{\equiv}CCH_2SiMe_3)^+$ (**8a**), **4a**, and free PTMS. The NMR data for **7a**,**b**,and **8a** are consistent with highly unsymmetrical substrate coordination and substantial polarization of the substrate multiple bond with significant positive charge buildup at C_{int} and negative charge buildup at C_{term}. PTMS binds to **4a** more strongly than ATMS does. The ATMS adducts undergo nondissociative alkene face exchange ("alkene flipping"), i.e., exchange of the $(C_5H_4R)_2Zr(C_6F_5)^+$ unit between the two alkene enantiofaces without decomplexation of the alkene, on the NMR time scale.

Introduction

Metallocene-catalyzed polymerization of alkenes occurs by a coordination−insertion mechanism via intermediate metal−alkyl−alkene species (Scheme 1).[1] Studies of discrete d^0 metal−(σ-carbyl)−alkene complexes would be very helpful in understanding this important process. However, due to weak alkene binding and low insertion barriers,[2] observation of these intermediates is exceedingly difficult, and instead, model complexes have been used to probe their properties.

Chelated d^0 metal−alkoxide−alkene complexes,[3] chelated d^0 metal−alkyl−alkene complexes,[4] and nonchelated d^0 metal−alkene complexes without σ-carbyl ligands are known.[5] The only reported nonchelated d^0 metal−alkyl−alkene complexes are the Cp^*_2YR(alkene) species (**A**; $Cp^* = C_5Me_5$; R = CH_2CH_2-

Scheme 1

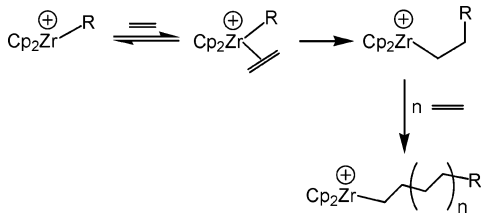

$CHMe_2$, CH_2CHMe_2, $CH_2(CH_2)_4Me$, cyclopentyl) described by Casey,[6] and the $[(indenyl)_2ZrMe][\eta^2$-indole·$B(C_6F_5)_3]$ ion pair (**B**) reported by Resconi,[7] which are shown in Chart 1. The yttrium−alkene adducts were not directly observed, but low-temperature NMR spectra of mixtures of Cp^*_2YR and alkene contained one set of exchange-averaged alkene resonances that are shifted in the same direction from the free alkene positions as for chelated yttrium−alkene complexes,[4a] indicating the reversible formation of Cp^*_2YR(alkene) adducts. These species undergo insertion above −100 °C, except when R = cyclopentyl. Here we describe the generation and properties of nonchelated d^0 Zr−aryl−alkene and −alkyne complexes.[8]

(1) (a) Cossee, P. *Tetrahedron Lett.* **1960**, *17*, 12. (b) Cossee, P. *J. Catal.* **1964**, *3*, 80. (c) Arlman, E. J.; Cossee, P. *J. Catal.* **1964**, *3*, 99. (d) Brookhart, M.; Green, M. L. H. *J. Organomet. Chem.* **1983**, *250*, 395. (e) Grubbs, R. H.; Coates, G. W. *Acc. Chem. Res.* **1996**, *29*, 85.
(2) (a) Margl, P.; Deng, L.; Ziegler, T. *Top. Catal.* **1999**, *7*, 187. (b) Fan, L.; Harrison, D.; Woo, T. K.; Ziegler, T. *Organometallics* **1995**, *14*, 2018. (c) Woo, T. K.; Fan, L.; Ziegler, T. *Organometallics* **1994**, *13*, 2252. (d) Lanza, G.; Fragalà, I. L. *Top. Catal.* **1999**, *7*, 45. (e) Lauher, J. W.; Hoffmann, R. *J. Am. Chem. Soc.* **1976**, *98*, 1729.
(3) (a) Carpentier, J. F.; Wu, Z.; Lee, C. W.; Strömberg, S.; Christopher, J. N.; Jordan, R. F. *J. Am. Chem. Soc.* **2000**, *122*, 7750. (b) Carpentier, J.-F.; Maryin, V. P.; Luci, J.; Jordan, R. F. *J. Am. Chem. Soc.* **2001**, *123*, 898. (c) Wu, Z.; Jordan, R. F.; Petersen, J. L. *J. Am. Chem. Soc.* **1995**, *117*, 5867.
(4) Leading references: (a) Casey, C. P.; Klein, J. F.; Fagan, M. A. *J. Am. Chem. Soc.* **2000**, *122*, 4320. (b) Casey, C. P.; Carpenetti, D. W., II. *Organometallics* **2000**, *19*, 3970. (c) Brandow, C. G.; Mendiratta, A.; Bercaw, J. E. *Organometallics* **2001**, *20*, 4253. (d) Casey, C. P.; Carpenetti, D. W., II; Sakurai, H. *Organometallics* **2001**, *20*, 4262. (e) Cano, J.; Gómez-Sal, P.; Heinz, G.; Martínez, G.; Royo, P. *Inorg. Chim. Acta* **2003**, *345*, 15. (f) Martínez, G.; Royo, P. *Organometallics* **2005**, *24*, 4782.
(5) (a) Witte, P. T.; Meetsma, A.; Hessen, B.; Budzelaar, P. H. M. *J. Am. Chem. Soc.* **1997**, *119*, 10561. (b) Humphries, M. J.; Douthwaite, R. E.; Green, M. L. H. *J. Chem. Soc., Dalton Trans.* **2000**, 2952. (c) Kress, J.; Osborn, J. A. *Angew. Chem., Int. Ed, Engl.* **1992**, *31*, 1585.
(6) (a) Casey, C. P.; Tunge, J. A.; Lee, T.-Y.; Fagan, M. A. *J. Am. Chem. Soc.* **2003**, *125*, 2641. (b) Casey, C. P.; Lee, T.-Y.; Tunge, J. A.; Carpenetti, D. W., II. *J. Am. Chem. Soc.* **2001**, *123*, 10762.
(7) (a) Bonazza, A.; Cumurati, I.; Guidotti, S.; Mascellari, N.; Resconi, L. *Macromol. Chem. Phys.* **2004**, *205*, 319. (b) For related species see: Kehr, G.; Fröhlich, R.; Wibbeling, B.; Erker, G. *Chem. Eur. J.* **2000**, *6*, 258.
(8) Preliminary communication: Stoebenau, E. J., III; Jordan, R. F. *J. Am. Chem. Soc.* **2004**, *126*, 11170.

10.1021/ja057524p CCC: $33.50

Chart 1

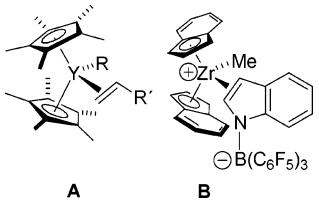

Results and Discussion

Targets. For this work, we were interested in systems in which alkene and alkyne coordination to a d^0 Zr−σ-carbyl complex could be studied in the absence of insertion reactions. A two-component strategy was used. First, to circumvent the problems posed by weak substrate binding, the β-Si-substituted substrates allyltrimethylsilane (ATMS) and propargyltrimethylsilane (PTMS) were used. These substrates coordinate strongly to $[Cp'_2Zr(O^tBu)][B(C_6F_5)_4]$ (**1**, Cp' = C_5H_4Me) due to β-Si stabilization of the partial positive charge at C_{int} of the bound substrates.[8] Second, to inhibit insertion, the electron-deficient, poorly nucleophilic pentafluorophenyl (C_6F_5) ligand was used as the σ-carbyl group.[9]

Neutral $(C_5H_4R)_2Zr(C_6F_5)R$ Compounds. The pentafluorophenyl compounds $Cp_2Zr(C_6F_5)_2$ (**2a**, Cp = C_5H_5),[10] $Cp_2Zr(C_6F_5)Me$ (**3a**),[11] and $Cp'_2Zr(C_6F_5)Me$ (**3b**) were synthesized by literature methods, as shown in Scheme 2.

Scheme 2

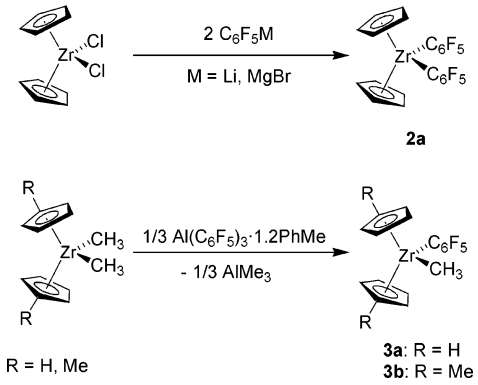

Reactivity of 2a. The reactions of **2a** with standard polymerization activators[12] were investigated to determine if Zr−C_6F_5 bond protonolysis or $C_6F_5^-$ anion abstraction could provide access to $Cp_2Zr(C_6F_5)^+$ species. Compound **2a** does not react with $[HNPh_2Me][B(C_6F_5)_4]$ in C_6D_5Cl at 22 °C, even after 4 days. This lack of reactivity was unexpected, as **3a**,**b** react with

Scheme 3. Anion = $B(C_6F_5)_4^-$

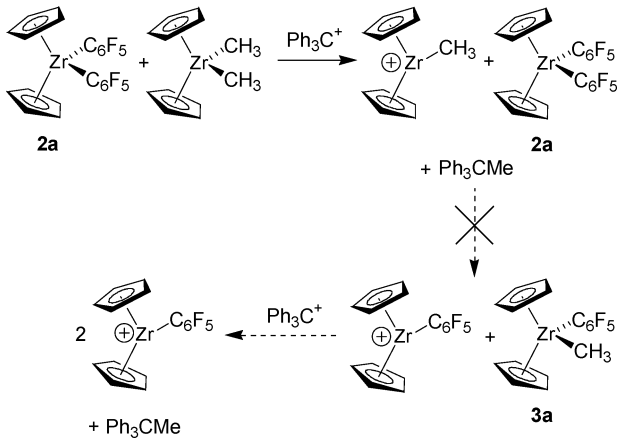

H_2O or D_2O to yield $\{(C_5H_4R)_2ZrMe\}_2(\mu\text{-}O)$[13] and C_6F_5H or C_6F_5D by selective reaction of the Zr−C_6F_5 bond. One explanation for this difference in reactivity is that initial coordination of H_2O to Zr facilitates proton transfer in the latter reaction.[14] Complex **2a** is also unreactive with $[Ph_3C][B(C_6F_5)_4]$ and with $B(C_6F_5)_3$ under these conditions.[15]

The reaction of **2a**, Cp_2ZrMe_2, and $[Ph_3C][B(C_6F_5)_4]$ in a 1:1:2 molar ratio was investigated to determine if $Cp_2Zr(C_6F_5)^+$ could be generated by the methide abstraction and ligand exchange process shown in Scheme 3. A similar approach was used for the synthesis of cationic Al alkyls.[16] However, this reaction generates only Cp_2ZrMe^+ and Ph_3CMe (1 equiv), along with unreacted **2a** and $[Ph_3C][B(C_6F_5)_4]$. Exchange of a C_6F_5 group from **2a** to Cp_2ZrMe^+ to generate $Cp_2Zr(C_6F_5)^+$ and **3a** is not observed.

Generation of $(C_5H_4R)_2Zr(C_6F_5)^+$ Species. The lack of C_6F_5 abstraction from **2a** suggested that selective methide abstraction from **3a** could provide access to $Cp_2Zr(C_6F_5)^+$ species. Indeed, **3a** reacts with 1 equiv of $[Ph_3C][B(C_6F_5)_4]$ in C_6D_5Cl at 22 °C to yield $[Cp_2Zr(C_6F_5)][B(C_6F_5)_4]$ (**4a**, 97%, Scheme 4) after 2 days. At shorter reaction times, mixtures of **4a**, Ph_3CMe, Ph_3C^+, and the dinuclear species $[\{Cp_2Zr(C_6F_5)\}_2(\mu\text{-}Me)][B(C_6F_5)_4]$ (**5a**)[11] are observed. Compound **5a** forms by trapping of the initially generated **4a** by **3a** (Scheme 4). Compound **4a** could not be isolated, but rather was generated and used in situ. Similarly, the reaction of **3b** with $[Ph_3C][B(C_6F_5)_4]$ provides $[Cp'_2Zr(C_6F_5)][B(C_6F_5)_4]$ (**4b**, 93%, Scheme 4). Complex **4b** forms within 30 min, and no intermediates are observed in the reaction.

The difference in the rate of formation of **4b** vs **4a** reflects the difference in stabilities of $[\{Cp'_2Zr(C_6F_5)\}_2(\mu\text{-}Me)][B(C_6F_5)_4]$ (**5b**) and **5a**. When **3b** is treated with 0.5 equiv of $[Ph_3C][B(C_6F_5)_4]$ in C_6D_5Cl at 22 °C, an equilibrium mixture of **3b**, **4b**, and **5b** is obtained. The NMR signals for all three species are broad, implying that these species undergo intermolecular exchange on the NMR time scale. The equilibrium constant for formation of **5b** from **3b** and **4b** is $K_1 = [\mathbf{5b}][\mathbf{4b}]^{-1}[\mathbf{3b}]^{-1} = 410(20)\ M^{-1}$ (Scheme 4), as determined by ^1H NMR spectroscopy. In contrast, **5a** is formed *quantitatively* from **3a** and 0.5

(9) For M−C_6F_5 species, especially d^0 compounds, see: (a) Chambers, R. D.; Chivers, T. *Organomet. Chem. Rev.* **1966**, *1*, 279. (b) Alonso, P. J.; Favello, L. R.; Forniés, J.; García-Monforte, M. A.; Menjón, B. *Angew. Chem., Int. Ed.* **2004**, *43*, 5225. (c) Deacon, G. B.; Forsyth, C. M. *Organometallics* **2003**, *22*, 1349. (d) Hauber, S.-O.; Lissner, F.; Deacon, G. B.; Niemeyer, M. *Angew. Chem., Int. Ed.* **2005**, *44*, 5871. (e) Hauber, S.-O.; Lissner, F.; Deacon, G. B.; Niemeyer, M. *Angew. Chem., Int. Ed.* **2005**, *44*, 5871. (f) Maron, L.; Werkema, E. L.; Perrin, L.; Eisenstein, O.; Andersen, R. A. *J. Am. Chem. Soc.* **2005**, *127*, 279. For M−C_6Cl_5 species, see: (g) Ara, I.; Forniés, J.; García-Monforte, M. A.; Martín, A.; Menjón, B. *Chem. Eur. J.* **2004**, *10*, 4186.

(10) (a) Dioumaev, V. K.; Harrod, J. F. *Organometallics* **1997**, *16*, 2798. (b) Chaudhari, M. A.; Stone, F. G. A. *J. Chem. Soc. A* **1966**, 838. (c) Coe, P. L.; Stephens, R.; Tatlow, J. C. *J. Chem. Soc.* **1962**, 3227.

(11) Bochmann, M.; Sarsfield, M. J. *Organometallics* **1998**, *17*, 5908.

(12) Chen, E. Y.-X.; Marks, T. J. *Chem. Rev.* **2000**, *100*, 1391 and references therein.

(13) For $(Cp_2ZrMe)_2(\mu\text{-}O)$ see: Marsella, J. A.; Folting, K.; Huffman, J. C.; Caulton, K. G. *J. Am. Chem. Soc.* **1981**, *103*, 5596.

(14) Hillhouse, G. L.; Bercaw, J. E. *J. Am. Chem. Soc.* **1984**, *106*, 5472.

(15) For use of $B(C_6F_5)_3$ as a $C_6F_5^-$ abstracting agent, see: Forniés, J.; Martín, A.; Martín, L. F.; Menjón, B.; Tsipis, A. *Organometallics* **2005**, *24*, 3539.

(16) Korolev, A. V.; Ihara, E.; Guzei, I. A.; Young, V. G., Jr.; Jordan, R. F. *J. Am. Chem. Soc.* **2001**, *123*, 8291.

Scheme 4. Anion = $B(C_6F_5)_4^-$

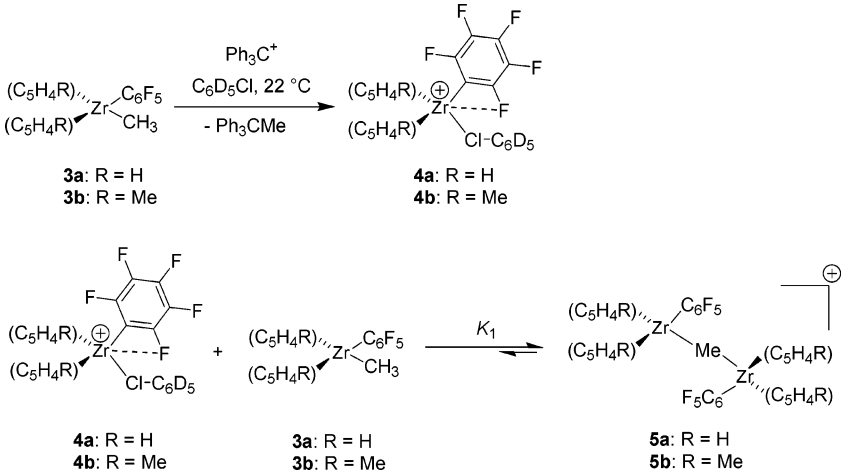

equiv of Ph_3C^+ under these conditions, implying that K_1 is much larger in this case (>5000 M^{-1}).[11] Cation **4a** is expected to be a stronger Lewis acid than **4b** due to the weaker donor ability of the Cp ligands compared to that of the Cp' ligands.[17] The greater Lewis acidity of **4a** vs **4b**, and the additional steric crowding present in **5b** vs **5a**, may explain the greater stability of **5a** vs **5b**.

Compound **4a** is stable in C_6D_5Cl solution for weeks at 22 °C, but decomposes rapidly in CD_2Cl_2, even at −78 °C ($t_{1/2}$ < 30 min), to C_6F_5H, C_6F_5D, [{$Cp_2Zr(C_6F_5)$}$_2$(μ-Cl)][$B(C_6F_5)_4$] (**6a**), and other Cp_2Zr species. Compound **6a** was generated independently by the reaction of **4a** with 0.5 equiv of [Bu_3NCH_2Ph]Cl. Compound **4b** exhibits stability similar to that of **4a**.

Solution Structure of $(C_5H_4R)_2Zr(C_6F_5)^+$. The ^{19}F NMR spectrum of **4b** at −38 °C contains two broad *o*-F resonances at δ −116.7 and −140.7, a sharp *p*-F triplet resonance, and two broad *m*-F resonances, as shown in Figure 1. The downfield *o*-F signal of **4b** is in the normal range for Zr−C_6F_5 compounds (δ −116 ± 10),[11,18] while the upfield *o*-F signal is 20−25 ppm upfield from the normal range. These results show that the sides of the C_6F_5 ligand are inequivalent and suggest that the *o*-F with the upfield resonance is datively coordinated to Zr. Dative *o*-CF···Zr interactions have been detected in other Zr−C_6F_5 complexes.[18a] In contrast, neutral Zr−C_6F_5 compounds that lack dative *o*-CF···Zr interactions but undergo slow Zr−C_6F_5 rotation typically display small (1−3 ppm) chemical shift differences between their *o*-F resonances.[18b,19] The ^{19}F NMR spectrum of **4a** is similar to that of **4b** under these conditions.

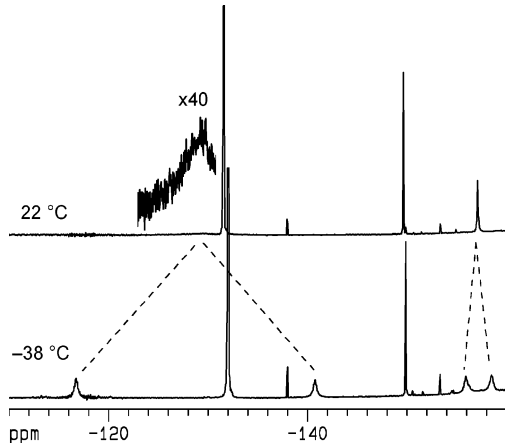

Figure 1. Variable temperature ^{19}F NMR spectra (471 MHz) of **4b**. Assignments for −38 °C spectrum: δ −117 (**4b** *o*-F), −132 (anion *o*-F), −138 (C_6F_5H *o*-F), −141 (**4b** *o*-F), −150 (**4b** *p*-F), −154 (C_6F_5H), −156 (**4b** *m*-F), −159 (**4b** *m*-F). The dashed lines highlight the coalescence of the two *o*-F and the two *m*-F resonances of **4b**.

Addition of bromobenzene (11 equiv) to a C_6D_5Cl solution of **4a** results in several changes in the NMR spectra at −38 °C. The ^{1}H NMR Cp resonance of **4a** is shifted downfield by 0.03 ppm, and the *p*-F signal of **4a** is broadened by 15−20 Hz, compared to spectra in the absence of PhBr. Additionally, the ^{13}C NMR resonances of PhBr are broadened by 2−6 Hz compared to resonances for Ph_3CMe, but are not shifted from the normal PhBr positions. These effects are ascribed to minor formation of a PhBr adduct that exchanges rapidly with **4a** and free PhBr and suggest that **4a**,**b** exist as solvent adducts in halocarbon solution. Zirconium−ClPh and −BrPh complexes are well characterized.[5a,b,20] The structure for **4a**,**b** proposed in Scheme 4, in which the *o*-CF···Zr interaction occupies the central coordination site, is based on the solid-state structure of Cp*$_2$Zr(κ^2-*C*,*Cl*-*o*-Cl-phenyl)(NCMe)$^+$.[20a]

Dynamics of $(C_5H_4R)_2Zr(C_6F_5)^+$ Species. The ^{19}F NMR spectrum of **4b** at 22 °C contains one very broad *o*-F resonance, a sharp *p*-F triplet resonance, and a slightly broad *m*-F resonance, as shown in Figure 1. Two dynamic processes could produce the observed coalescence of the *o*-F signals and of the *m*-F signals: rotation around the Zr−C_6F_5 bond of **4b**,[21] or site epimerization at Zr (i.e. exchange of the C_6F_5 and ClPh ligands between the sides of the zirconocene wedge, probably by exchange of free and coordinated PhCl), as shown in Scheme 5. Zr−C_6F_5 bond rotation permutes the sides of the C_6F_5 ring, while site epimerization permutes the sides of the C_6F_5 ring *and* the sides of the Cp' rings.

The ^{13}C{^{1}H} NMR spectrum of **4b** at −38 °C in C_6D_5Cl contains three broad Cp' CH resonances (Figure 2), one sharp Cp' ipso-C resonance, and one sharp Cp'*Me* resonance. The

(17) Wieser, U.; Babushkin, D.; Brintzinger, H.-H. *Organometallics* **2002**, *21*, 920.
(18) (a) Pindado, G. J.; Lancaster, S. J.; Thornton-Pett, M.; Bochmann, M. *J. Am. Chem. Soc.* **1998**, *120*, 6816. (b) Kraft, B. M.; Jones, W. D. *J. Organomet. Chem.* **2002**, *658*, 132.
(19) Edelbach, E. L.; Rahman, A. K. F.; Lachicotte, R. J.; Jones, W. D. *Organometallics* **1999**, *18*, 3170.
(20) (a) Wu, F.; Dash, A. K.; Jordan, R. F. *J. Am. Chem. Soc.* **2004**, *126*, 15360. (b) Bochmann, M.; Jaggar, A. J.; Nicholls, J. C. *Angew. Chem., Int. Ed. Engl.* **1990**, *29*, 780.
(21) Leblanc, J. C.; Moïse, C. *Org. Magn. Reson.* **1980**, *14*, 157.

Scheme 5

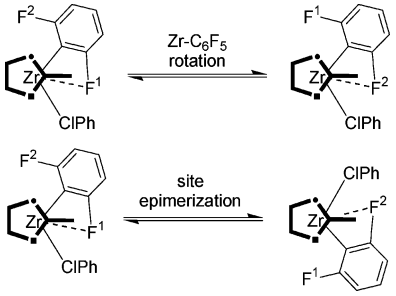

Cp' CH resonances collapse to two sharp singlets at 22 °C (Figure 2). The ^{1}H NMR spectrum of **4b** at −38 °C in C_6D_5Cl contains two broad Cp' CH resonances, which sharpen at 22 °C. These results show that the sides of the Cp' ligands are indeed exchanging rapidly on the NMR time scale, which implies that site epimerization of **4b** is rapid. The site epimerization barrier is $\Delta G^{\ddagger} = 11.2(1)$ kcal/mol at −38 °C, as estimated from the line broadening of the *o*-F and *m*-F resonances of **4b**.

It is also possible that Zr−C_6F_5 bond rotation occurs independently of the site epimerization process. If Zr−C_6F_5 bond rotation occurred at a rate that is competitive with the site epimerization rate, the *o*-F and *m*-F resonances of **4b** would exhibit greater exchange line broadening than the Cp' CH resonances in the slow-exchange region. However, at −38 °C, the excess line widths of the noncoalesced ^{13}C Cp' CH resonances and the ^{19}F *o*-F and *m*-F resonances are approximately equal (ca. 200 Hz). Therefore, Zr−C_6F_5 bond rotation in **4b** does not occur at a significant rate at this temperature.

The variable-temperature ^{19}F NMR spectra of **4a** are similar to those of **4b**, and it is likely that site epimerization occurs in this case as well.

Generation of Alkene and Alkyne Complexes of $(C_5H_4R)_2$-Zr$(C_6F_5)^+$. The addition of excess allyltrimethylsilane (ATMS) to **4a**,**b** results in the formation of equilibrium mixtures of **4a**,**b**, free ATMS, and the alkene adducts $[(C_5H_4R)_2Zr(C_6F_5)$-$(H_2C{=}CHCH_2SiMe_3)][B(C_6F_5)_4]$ (**7a**: R = H; **7b**: R = Me), as shown in eq 1. In a typical experiment, ATMS was added by vacuum transfer to a frozen solution of **4a**,**b** in C_6D_5Cl in an NMR tube. The tube was thawed, stored at −40 °C, and transferred to a precooled NMR probe with minimal transfer time (<1 min). This procedure minimized side reactions such as the dimerization of ATMS (vida infra). The propargyltrimethylsilane (PTMS) complex $[Cp_2Zr(C_6F_5)(HC{\equiv}CCH_2SiMe_3)]$-$[B(C_6F_5)_4]$ (**8a**) was generated in an analogous manner. Compounds **7a**,**b** and **8a** were characterized by NMR spectroscopy. These compounds are very thermally sensitive, which precluded isolation or ESI-MS analysis.

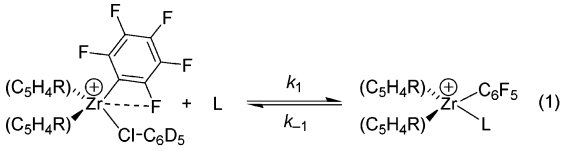

(1)

4a: R = H
4b: R = Me

cpd	R	L
7a	H	$H_2C{=}CHCH_2SiMe_3$
7b	Me	$H_2C{=}CHCH_2SiMe_3$
8a	H	$HC{\equiv}CCH_2SiMe_3$

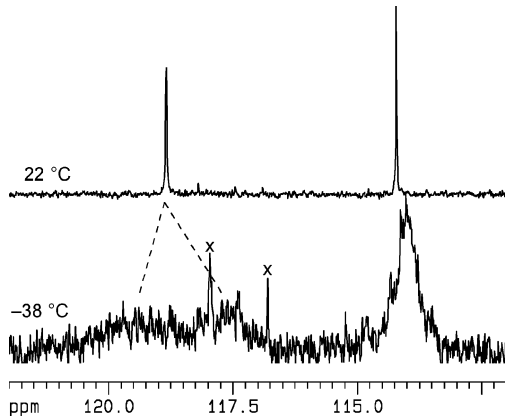

Figure 2. Partial variable temperature $^{13}C\{^1H\}$ NMR spectra (126 MHz) of **4b** showing the Cp' CH resonances. The dashed lines highlight the coalescence of two of the Cp' CH resonances. The peaks marked "x" are due to minor unknown impurities.

Table 1. NMR Coordination Shifts ($\Delta\delta$) for the ATMS Ligands in Zr^{IV} Compounds[a]

cmpd	$\Delta\delta$ C_{int}	$\Delta\delta$ C_{term}	$\Delta\delta$ $C_{allylic}$	$\Delta\delta$ H_{int}	$\Delta\delta$ H_{trans}	$\Delta\delta$ H_{cis}
7a	51.2	−15.4	12.2	1.89	−0.79	−1.01
7b	49.6	−15.2	11.9	1.90	−0.72	−0.85
9	32.0	−20.7	8.8	1.59	−0.35	−0.43

[a] In C_6D_5Cl at −38 °C; $\Delta\delta = \delta_{coord} - \delta_{free}$.

2-Butyne does not coordinate to **4a** in C_6D_5Cl at −38 °C, even though it coordinates strongly to **1** under these conditions. Therefore, simple alkenes such as ethylene or propylene are not expected to bind to **4a**, since these substrates bind much more weakly to **1** compared to 2-butyne. Side reactions precluded detection of binding of other substrates to **4a**,**b**. For example, while *tert*-butyl vinyl ether is expected to bind strongly, based on the strong coordination of this substrate to **1**, it is rapidly polymerized in the presence of **4a**, presumably by a cationic mechanism.

NMR Properties and Solution Structures of $(C_5H_4R)_2Zr$-$(C_6F_5)(ATMS)^+$ Species. The ^{1}H and $^{13}C\{^1H\}$ NMR spectra of **7a** at −38 °C in C_6D_5Cl each contain two Cp resonances, indicative of C_1 symmetry as expected due to the chiral center at C_{int} of the ATMS ligand. Additionally, these spectra each contain one set of resonances for the bound ATMS, consistent with the presence of one rotamer or with rapid rotation around the Zr−(alkene centroid) axis.[22] The ^{19}F NMR spectrum of **7a** contains one *p*-F resonance and one broad *m*-F resonance, but the *o*-F resonance is broadened into the baseline. This result shows that rotation around the Zr−C_6F_5 bond occurs on the NMR time scale in this species.[23] The NMR spectra of **7b** are similar to those of **7a**. The −38 °C ^{19}F NMR spectrum of **7b** contains two broad *o*-F resonances in the normal range for Zr−C_6F_5 compounds, consistent with κ^1-C_6F_5 coordination.

The ATMS ligands of **7a**,**b** display characteristic ^{13}C NMR coordination shifts ($\Delta\delta = \delta_{coord} - \delta_{free}$), which are listed in Table 1. The C_{int} resonances of **7a**,**b** are shifted ca. 50 ppm downfield, and the C_{term} resonances are shifted ca. 15 ppm

(22) These ligands probably undergo free rotation around the Zr−(ligand centroid) axis, based on the observation of fast rotation in $Cp'_2Zr(O^tBu)$-$(Me{\equiv}CMe)^+$ above −59 °C in CD_2Cl_2. Stoebenau, E. J., III; Jordan, R. F. *J. Am. Chem. Soc.* **2003**, *125*, 3222.

(23) Site epimerization of **7a** can be discounted because net exchange of free and coordinated ATMS is significantly slower than the exchange of the sides of the C_6F_5 ring (vida infra).

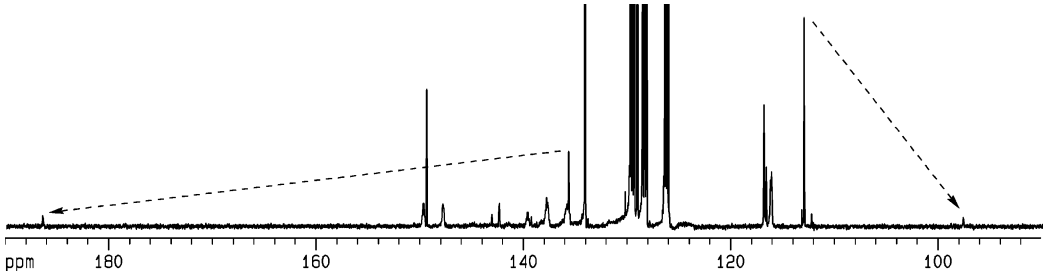

Figure 3. Partial $^{13}C\{^1H\}$ NMR spectrum of an equilibrium mixture of **7a**, **4a**, and free ATMS in C_6D_5Cl at −38 °C. ATMS coordination shifts are shown with dashed arrows. Assignments: δ 187 (**7a** C_{int}), 149 (Ph_3CMe), 149 (d, anion), 139 (d, anion), 137 (d, anion), 135 (ATMS C_{int}), 134−126 (large, C_6D_5Cl and Ph_3CMe), 125 (br, anion), 117 (2 s, **4a** and **6a** Cp), 116 (br 2 s, **7a** Cp), 113 (ATMS C_{term}), 98 (**7a** C_{term}).

upfield from the free ATMS resonances. The $^{13}C\{^1H\}$ NMR spectrum of **7a** is shown in Figure 3. The $^1J_{CH}$ values for C_{int} (161 Hz) and C_{term} (150 Hz) of **7a** are not significantly perturbed by coordination. The $C_{allylic}$ resonances of **7a**,**b** are shifted ca. 12 ppm downfield from the free alkene value.

The ^1H NMR resonances of the ATMS vinyl unit of **7a**,**b** are also perturbed by coordination (Table 1). The H_{int} resonances shift 1.9 ppm downfield, and the H_{trans} and H_{cis} resonances shift 0.7−1.0 ppm upfield from the free ATMS resonances. Two broad resonances for the diastereotopic $H_{allylic}$ hydrogens are observed for **7a**,**b**, which are shifted downfield by 0.7−1.0 ppm by coordination. The ATMS $^nJ_{HH}$ coupling constants for **7a** and **7b** are virtually unchanged from the free alkene values.

The NMR data for **7a**,**b** are generally similar to data for $[Cp'_2Zr(O^tBu)(H_2C{=}CHCH_2SiMe_3)][B(C_6F_5)_4]$ (**9**) and other Zr^{IV}−alkene complexes studied previously and thus imply the alkene is bound in an unsymmetrical, η^1-fashion (d(Zr−C_{int}) > d(Zr−C_{term})), which results in polarization of the C=C bond with partial positive charge on C_{int} and partial negative charge on C_{term}, but not significant rehybridization of the alkene carbons.[3,8] The larger $\Delta\delta$ values for C_{int} and H_{int} for **7a**,**b** compared to those for **9** suggest that the ATMS C=C bond may be more polarized in the former species than in the latter, i.e., that there is a greater contribution of the carbocationic resonance form in **7a**,**b** than in **9**. This difference is reasonable because the $(C_5H_4R)_2Zr(\kappa^1\text{-}C_6F_5)^+$ fragments in **7a**,**b** are expected to be stronger Lewis acids than the $Cp'_2Zr(O^tBu)^+$ fragment in **9**, due to the electron-withdrawing nature of the C_6F_5 group. In fact the $\Delta\delta$ values for C_{int} in **7a**,**b** are similar to that observed for $[(C_6F_5)_3BCH_2CH{=}CH_2][SnBu_3]$ (i.e., the $B(C_6F_5)_3$ adduct of $Bu_3SnCH_2CH{=}CH_2$; $\Delta\delta$ = 54), in which the carbocationic-C_{int} resonance form is believed to make a substantial contribution.[24]

An alternative formulation of **7a**,**b** as alkene insertion products, i.e., $(C_5H_4R)_2Zr\{CH_2CH(C_6F_5)CH_2SiMe_3\}^+$ or $(C_5H_4R)_2Zr\{CH(CH_2SiMe_3)CH_2C_6F_5\}^+$, is ruled out by NMR data and reactivity properties. The $^1J_{CH}$ values of **7a** are characteristic for sp^2 carbons and are too large for insertion products in which these carbons would be sp^3 hybridized. For example, $^1J_{CH}$ = 132 Hz for C_6F_5Me, which is a reasonable model for C_β of an insertion product. The $^1J_{CH}$ value for C_α of an insertion product would be even lower. Also, addition of THF to equilibrium mixtures of **7a** and **4a** at −38 °C results in fast (<5 min) quantitative formation of $[Cp_2Zr(C_6F_5)(THF)][B(C_6F_5)_4]$ (**10a**) and free ATMS, which would require that insertion be reversible on a fast time scale, which is unlikely.

(24) Blackwell, J. M.; Piers, W. E.; McDonald, R. *J. Am. Chem. Soc.* **2002**, *124*, 1295.

Table 2. NMR Coordination Shifts ($\Delta\delta$) and Coupling Constants (Hz) for the PTMS Ligands in Zr^{IV} Compounds[a]

cmpd	$\Delta\delta$ C_{int}	$\Delta\delta$ C_{term}	$\Delta\delta$ C_{prop}[b]	$\Delta\delta$ H_{term}	$\Delta\delta$ H_{prop}[b]	$^1J_{C\equiv CH}$	$^2J_{C\equiv CH}$
8a[c]	62.5	10.5	10.0	2.57	0.78	232	34
11[d]	21.7	−0.9	7.0	1.58	0.48	244	43

[a] $\Delta\delta = \delta_{coord} - \delta_{free}$. [b] $HC{\equiv}CCH_2R$ resonance. [c] In C_6D_5Cl solution, −38 °C. [d] In CD_2Cl_2 solution, −89 °C.

Moreover, as described below, **4a** and **7a** interconvert on the NMR time scale, which would also require rapid reversible insertion of ATMS.

NMR Properties and Solution Structure of $Cp_2Zr(C_6F_5)(HC{\equiv}CCH_2SiMe_3)^+$. The ^1H and $^{13}C\{^1H\}$ NMR spectra of PTMS adduct **8a** each contain one Cp resonance and one set of PTMS resonances, consistent with the presence of a single rotamer in which the PTMS ligand lies in the plane between the two Cp rings or with fast rotation around the Zr−(alkyne centroid) axis.[22] The ^{19}F NMR spectrum contains two broad *o*-F resonances in the normal range for $Zr{-}C_6F_5$ compounds,[18] a sharp *p*-F triplet resonance, and a broad *m*-F resonance, consistent with κ^1-C_6F_5 coordination and hindered $Zr{-}C_6F_5$ bond rotation on the NMR time scale.

The NMR data for **8a** are compared to those of $[Cp'_2Zr(O^tBu)(HC{\equiv}CCH_2SiMe_3)][B(C_6F_5)_4]$ (**11**) in Table 2. For **8a**, C_{int}, C_{prop}, and H_{term} all show large downfield coordination shifts, and the $\Delta\delta$ values for C_{int} and H_{term} are substantially larger than these values for **11** and other $Cp'_2Zr(O^tBu)(HC{\equiv}CR)^+$ compounds. In addition, the coordination shift for C_{term} of **8a** is downfield, while for **11** and similar species this coordination shift is always slightly upfield. Finally, the J_{CH} values of the alkyne carbons of **8a** are 10−15 Hz smaller than for **11**. The J_{CH} values for **8a** imply essentially sp hybridization at the alkyne carbons but suggest that there is some bending of the H−C≡C unit. These results are consistent with unsymmetrical PTMS coordination (d(Zr−C_{int}) > d(Zr−C_{term}); **C** in Figure 4) and concomitant polarization of the C≡C bond with positive charge buildup at C_{int} for both **8a** and **11**, but imply a greater degree of polarization in **8a** than in **11**. In fact, the PTMS ligand of **8a** may possesses moderate vinyl cation character (**D** and **E**, Figure 4), as the ^{13}C NMR C_{int} resonance of **8a** (δ 145) is shifted more than halfway from the free PTMS value (δ 83) to values for silyl- and ferrocenyl-stabilized vinyl cations (δ_C 180−200).[25]

(25) (a) Müller, T.; Juhasz, M.; Reed, C. A. *Angew. Chem, Int. Ed.* **2004**, *43*, 1543. (b) Müller, T.; Meyer, R.; Lennartz, D.; Siehl, H.-U. *Angew. Chem., Int. Ed.* **2000**, *39*, 3074. (c) Koch, E.-W.; Siehl, H.-U.; Hanack, M. *Tetrahedron Lett.* **1985**, *26*, 1493. (d) Siehl, H.-U.; Kaufmann, F.-P.; Apeloig, Y.; Braude, V.; Danovich, D.; Berndt, A.; Stamatis, N. *Angew. Chem., Int. Ed. Engl.* **1991**, *30*, 1479. (e) Müller, T.; Margraf, D.; Syha, Y. *J. Am. Chem. Soc.* **2005**, *127*, 10852.

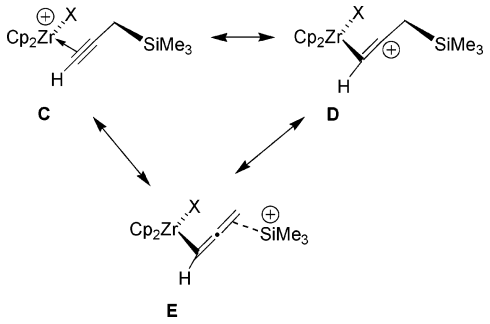

Figure 4. Polarization of the C≡C bond in **8a** (X = C_6F_5) and **11** (X = O^{t}Bu) showing a contribution from β-Si-stabilized vinyl cation canonical forms (**D** and **E**).

Table 3. Equilibrium Constants (K_{eq}) for Binding of ATMS and PTMS (L) in $(C_5H_4R)_2Zr(X)(L)^+$[a]

cmpd	formula	K_{eq} (M^{-1})
8a	$Cp_2Zr(C_6F_5)(HC{\equiv}CCH_2SiMe_3)^+$	910(60)
7a	$Cp_2Zr(C_6F_5)(H_2C{=}CHCH_2SiMe_3)^+$	8.2(1.4)
9	$Cp'_2Zr(O^tBu)(H_2C{=}CHCH_2SiMe_3)^+$	2.9(7)
7b	$Cp'_2Zr(C_6F_5)(H_2C{=}CHCH_2SiMe_3)^+$	2.4(2)

[a] At −38 °C in C_6D_5Cl; $K_{eq} = [Zr\text{-}L][\mathbf{4}]^{-1}[L]^{-1}$.

The greater C≡C polarization in **8a** vs **11** again reflects the expected greater Lewis acidity of $Cp_2Zr(\kappa^1\text{-}C_6F_5)^+$ vs $Cp'_2Zr(O^tBu)^+$.

The NMR data and reactivity properties of **8a** are inconsistent with the alternative formulation of this species as an insertion product, i.e., $Cp_2Zr\{C(CH_2SiMe_3){=}CHC_6F_5\}^+$ or $Cp_2Zr\{CH{=}C(C_6F_5)CH_2SiMe_3\}^+$. The $^nJ_{CH}$ values of **8a** are far too large for an insertion product, in which these carbons would be sp^2 hybridized. For example, in 2,3,4,5,6-pentafluorostyrene, a reasonable model for the insertion products, the $^1J_{CH}$ values are typical for sp^2 carbons (C_{term}: 161 Hz, C_{int}: 163 Hz), and the $^2J_{CH}$ values are not resolvable (<2 Hz). Also, while **8a** exhibits coupling between C_{term} and the *o*-fluorines (J_{CF} = 8 Hz), such coupling is not expected in an insertion product since it is not detectable in 2,3,4,5,6-pentafluorostyrene. Finally, the PTMS ligand is readily displaced by THF yielding **10a** and free PTMS, which would require that insertion be rapidly reversible.

Thermodynamics of Alkene and Alkyne Binding to $(C_5H_4R)_2Zr(C_6F_5)^+$ Species. Equilibrium constants for substrate binding to **4a**,**b** in eq 1, $K_{eq} = [Zr{-}L][\mathbf{4}]^{-1}[L]^{-1}$, were determined by NMR spectroscopy and are listed in Table 3.[26]

The equilibrium constant for ATMS coordination in **7a** is K_{eq} = 8.2(1.4) M^{-1} at −38 °C in C_6D_5Cl solution. At $[\mathbf{4a}]_{initial}$ = 0.040 M and $[ATMS]_{initial}$ = 0.20 M, ca. 59% of the total $Cp_2Zr(C_6F_5)^+$ exists as **7a** under these conditions. This equilibrium constant is unchanged over the concentration ranges $[\mathbf{4a}]_{initial}$ = 0.023−0.064 M and $[ATMS]_{initial}$ = 0.11−2.10 M. As the temperature is raised, the formation of **7a** becomes less favored, and the equilibrium shifts to **4a** and free ATMS. A van't Hoff analysis for ATMS coordination to **4a** (Figure 5) gives $\Delta H° = -5.3(2)$ kcal/mol and $\Delta S° = -18(1)$ eu.[26] The $\Delta H°$ value shows that the Zr−ATMS bond of **7a** is ca. 5 kcal/mol stronger than the sum of the Zr−ClC_6D_5 and *o*-CF···Zr bonds of **4a**.

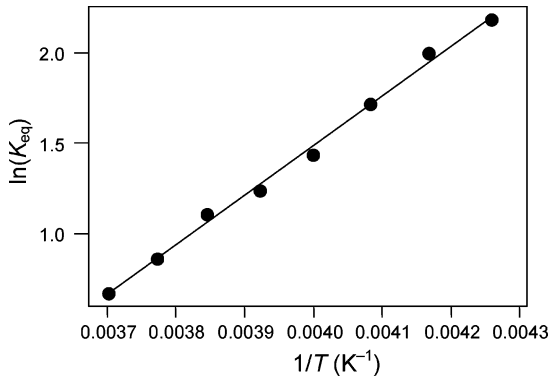

Figure 5. van't Hoff plot for ATMS coordination in **7a** in C_6D_5Cl.

The K_{eq} value for binding of ATMS in **7b** is ca. 3.5 times lower than that for **7a**, consistent with the weaker Lewis acidity of **4b** compared to **4a**.[17] There is no significant difference in the K_{eq} values for **7b** and **9**, even though $Cp'_2Zr(\kappa^1\text{-}C_6F_5)^+$ is expected to be a stronger Lewis acid than $Cp'_2Zr(O^tBu)^+$. However, the formation of **7b** from **4b** requires cleavage of the dative *o*-CF···Zr interaction *and* the Zr−ClPh bond, while the formation of **9** from **1** requires *only* cleavage of the Zr−ClPh bond.

The K_{eq} value for binding of PTMS in **8a** is 110 times higher than that for ATMS binding in **7a**, consistent with the trend observed for $Cp'_2Zr(O^tBu)(substrate)^+$ species, in which alkyne coordination is normally stronger than alkene coordination. At $[\mathbf{4a}]_{initial}$ = 0.054 M and $[PTMS]_{initial}$ = 0.061 M, ca. 91% of the total $Cp_2Zr(C_6F_5)^+$ exists as **8a** at −38 °C in C_6D_5Cl. The K_{eq} value for **8a** cannot be directly compared to that for **11** since PTMS binds too strongly to $Cp'_2Zr(O^tBu)^+$ under these conditions (C_6D_5Cl, −38 °C) for K_{eq} to be measured in this case. However, K_{eq} for formation of **11** is estimated to be greater than 1200 M^{-1}, and so the K_{eq} for formation of **8a** is less than that for **11**.

Intermolecular Alkene Exchange. The NMR resonances of an equilibrium mixture of **7a**, **4a**, and free ATMS in C_6D_5Cl solution broaden as the temperature is raised above −38 °C. The ^1H Cp resonance of **7a** coalesces with that of **4a** at ca. −12 °C, while the ^{13}C $SiMe_3$ resonance of **7a** coalesces with that of free ATMS at ca. −18 °C. The other resonances of **7a** are extremely broad at 2 °C but are not coalesced with those of **4a** or free ATMS at this temperature. Study of this system in the fast-exchange regime was difficult due to the lopsided equilibrium above 0 °C. These dynamic effects are consistent with the exchange of **7a** with **4a** and of coordinated ATMS with free ATMS.

Several observations show that the bound ATMS in **7a** is *not* directly displaced by free ATMS (Scheme 6; direct alkene exchange can result in retention or inversion of configuration at C_{int}). First, the H_{trans} and *p*-F NMR signals of **7a** show equal excess line broadening between −38 and +2 °C,[27] whereas direct associative alkene exchange would cause greater broadening of the former signal than the latter, as H_{trans} of **7a** exchanges environments in this process while *p*-F of **7a** does not. Second, the line widths of the H_{trans} and *p*-F signals of **7a** are independent of the concentration of free ATMS over the concentration range

(26) If the solvent term is included, the equilibrium constant for eq 1 is $K_{eq}' = K_{eq}[C_6D_5Cl]$, where K_{eq} is defined as in the text. If the solvent concentration is assumed to be independent of temperature, the value of $\Delta H°$ is not affected, but the entropy term becomes $\Delta S'° = \Delta S° + R\ln[C_6D_5Cl]$, where $R\ln[C_6D_5Cl] \approx 4.5$ eu.

(27) The difference in excess line widths of the H_{trans} and *p*-F resonances of **7a** showed no trend with temperature and averaged 1.2 Hz between −38 and +2 °C.

Scheme 6

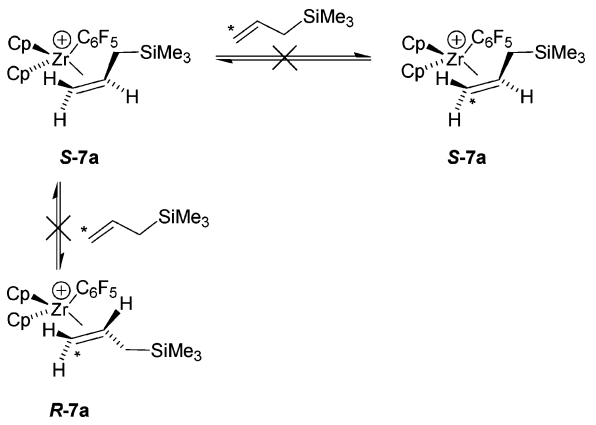

[ATMS] = 0.083−0.18 M. These results imply that ATMS is lost from **7a** to give **4a**, and free ATMS displaces C_6D_5Cl from **4a** to give **7a** (eq 1).

First-order rate constants for ATMS decomplexation from **7a** (k_{-1} in eq 1) were determined from the excess line broadening of the H_{trans} and *p*-F signals of **7a** between −38 and +2 °C. The line broadening data give k_{-1} = 5.5(2.5) s^{-1} at −38 °C in C_6D_5Cl. A ^{1}H EXSY NMR spectrum under the same conditions contains cross-peaks between the free and coordinated ATMS resonances and gives k_{-1} = 5.1(1) s^{-1},[28] in close agreement with the result from the line broadening data.

An Eyring analysis for ATMS decomplexation from **7a** (Figure 6) gives $\Delta H_{-1}^{\ddagger}$ = 8.9(6) kcal/mol and $\Delta S_{-1}^{\ddagger}$ = −17-(3) eu. The negative entropy of activation is consistent with displacement of ATMS from **7a** by C_6D_5Cl in an associative process. An incipient *o*-CF···Zr interaction in the transition state may also contribute to the negative entropy of activation.

The ATMS decomplexation rate constant for **7b**, k_{-1} = 12-(5) s^{-1} at −38 °C in C_6D_5Cl, was determined from the excess line broadening of the H_{trans} and *p*-F NMR signals of **7b**. The excess line widths of these two signals are very similar, discounting the occurrence of direct alkene exchange between **7b** and free ATMS. The slightly faster ATMS decomplexation rate for **7b** vs **7a** is consistent with the slightly weaker ATMS binding in **7b** vs **7a** (Table 3). Remarkably, ATMS decomplexation from **7b** is ca. 10 times slower than for the O^{t}Bu analogue **9** (k_{-1} = 125(25) s^{-1} at −38 °C in C_6D_5Cl), even though the K_{eq} values are similar for these systems. This difference may

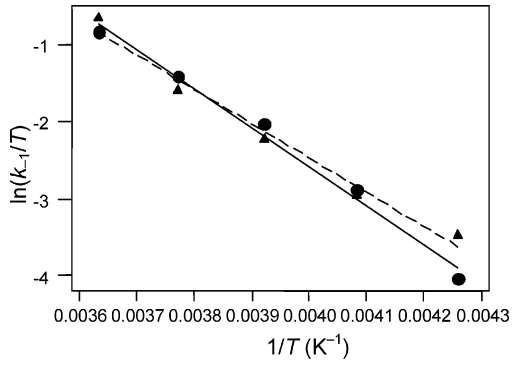

Figure 6. Eyring plot for ATMS decomplexation (k_{-1}) from **7a**. The plot of circles (solid line) is from H_{trans} NMR line broadening data. The plot of triangles (dashed line) is from *p*-F NMR line broadening data.

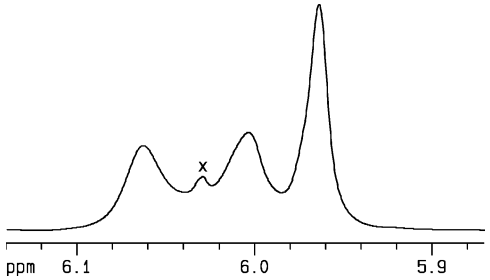

Figure 7. Partial ^{1}H NMR spectrum (500 MHz) of an equilibrium mixture of **7a** (0.034 M), **4a** (0.024 M), and free ATMS (0.17 M) at −38 °C in C_6D_5Cl, showing the greater line widths for the Cp signals of **7a** at δ 6.06 (ω = 14 Hz) and 6.00 (ω = 12 Hz) compared to that of **4a** at δ 5.97 (ω = 6 Hz). The minor resonance labeled "x" is due to an unknown impurity.

be due to greater lateral steric crowding in the metallocene wedge of **7b** compared to that in **9**, which restricts entry of solvent.

Dynamics of $(C_5H_4R)_2Zr(C_6F_5)(ATMS)^+$ Complexes. Selective NMR line broadening effects suggested that **7a** may undergo an *intramolecular* dynamic process in addition to the intermolecular exchange process in eq 1. First, for the dynamic equilibrium in eq 1, it is expected that the exchange broadening of the NMR resonances in the slow-exchange region of **4a** will be greater than that for **7a** when [**4a**] < [**7a**].[29] However, the ^{1}H NMR line widths of the Cp signals of **7a** are greater than the Cp signal of **4a** under these conditions (Figure 7). Second, the $H_{allylic}$ and Cp resonances of **7a** exhibit greater exchange broadening than the other resonances of **7a** in the slow-exchange region. Third, the excess broadening of the $H_{allylic}$ and Cp signals of **7a** is independent of [ATMS]. These data imply that **7a** undergoes an intramolecular process that permutes the two diastereotopic Cp rings, and the two diastereotopic allylic hydrogens. The simplest such process is nondissociative alkene enantioface exchange ("alkene flipping"),[30] i.e., exchange of the $Cp_2Zr(C_6F_5)^+$ unit between the two ATMS enantiofaces without decomplexation of the ATMS ligand, as shown in eq 2.

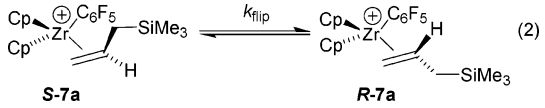

(2)

The rate constant for alkene flipping in **7a**, determined from the greater excess line broadening of the downfield $H_{allylic}$ signal compared to that of the H_{trans} signal, is k_{flip} = 18(1) s^{-1} (C_6D_5Cl, −38 °C). The EXSY spectrum of an equilibrium mixture of **7a**, **4a**, and ATMS (Figure 8) contains cross-peaks between the two $H_{allylic}$ resonances of **7a**,[31] which are larger than those between the $H_{allylic}$ resonances of **7a** and **4a**, confirming that alkene flipping occurs in **7a**. Analysis of the EXSY spectrum

(28) (a) Perrin, C. L.; Dwyer, T. J. *Chem. Rev.* **1990**, *90*, 935. (b) Johnston, E. R.; Dellwo, M. J.; Hendrix, J. *J. Magn. Reson.* **1986**, *66*, 399. (c) Perrin, C. L.; Gipe, R. K. *J. Am. Chem. Soc.* **1984**, *106*, 4036.

(29) At equilibrium for eq 1, k_1[**4a**][ATMS] = k_{-1}[**7a**] (equal rates). Under slow NMR exchange conditions, the excess line width due to exchange is $\Delta\omega = \omega - \omega_0$, where ω is the line width at half-height of a given resonance and ω_0 is its line width in the absence of exchange. For **4a**, $\Delta\omega_{4a} = k_1$-[ATMS]/π and for **7a**, $\Delta\omega_{7a} = k_{-1}/\pi$. Therefore, if eq 1 is the only exchange process, at equilibrium, by simple substitution $\Delta\omega_{4a}$[**4a**] = $\Delta\omega_{7a}$[**7a**]. Thus, if [**4a**] < [**7a**], then $\Delta\omega_{4a} > \Delta\omega_{7a}$, and if the line widths in the absence of exchange are approximately equal, then $\omega_{4a} > \omega_{7a}$.

(30) The nomenclature of this process is from: Prosenc, M.-H.; Brintzinger, H.-H. *Organometallics* **1997**, *16*, 3889.

(31) Under the mixing times used, dipole−dipole interactions do not contribute significantly to the cross-peak volumes, as is evident from the absence of cross-peaks between H_{cis} and H_{trans} of **7a**.

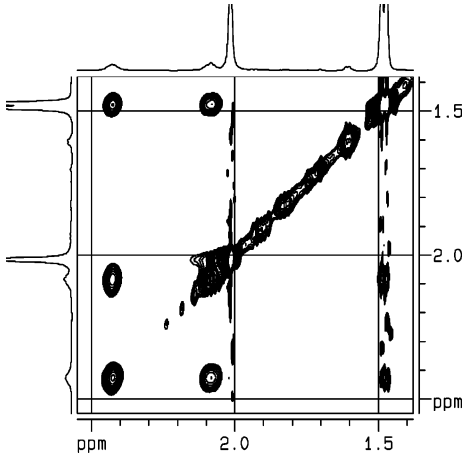

Figure 8. ^{1}H 2D EXSY NMR spectrum of an equilibrium mixture of **7a**, **4a**, and free ATMS. The $H_{allylic}$ region is shown. The $H_{allylic}$ signals of **7a** occur at δ 2.41 (br) and 2.07 (br), while that for free ATMS occurs at δ 1.44. The resonance at δ 2.01 is the Ph_3CMe resonance.

Table 4. First-Order Rate Constants and Free Energy Barriers for ATMS Decomplexation (k_{-1}, $\Delta G_{-1}^{\ddagger}$) and Alkene Flipping (k_{flip}, $\Delta G_{flip}^{\ddagger}$) for ATMS Complexes[a]

cmpd	k_{-1} (s^{-1})	$\Delta G_{-1}^{\ddagger}$(kcal/mol)	k_{flip} (s^{-1})	$\Delta G_{flip}^{\ddagger}$ (kcal/mol)
7a (1b)[b]	5.5(2.5)	12.8(2)	18(1)	12.3(1)
7a (EXSY)[c]	5.1(1)	12.9(1)	23.0(3)	12.2(1)
7b (lb)[b]	12(5)	12.5(2)	290(80)	11.0(1)
9 (lb)[b]	125(25)	11.4(1)	–	–

[a] In C_6D_5Cl at −38 °C. [b] Determined from NMR line broadening data. [c] Determined from EXSY NMR spectroscopy.

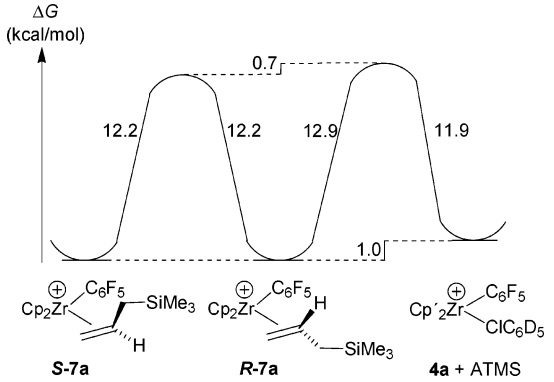

Figure 9. Free energy diagram comparing alkene flipping and alkene decomplexation from **7a** in C_6D_5Cl solution at −38 °C.

gives k_{flip} = 23.0(3) s^{-1} (C_6D_5Cl, −38 °C) for **7a**, in good agreement with the value found by NMR line broadening. Thus, alkene flipping is ca. 4 times faster than alkene decomplexation in **7a** (Table 4). The energetics of alkene flipping and decomplexation of **7a** are compared in the free energy diagram in Figure 9.[32]

Compound **7b** also undergoes alkene flipping, as is evident from the greater excess line broadening of the $H_{allylic}$ NMR signals compared to the other ATMS resonances for this species. The rate constant for alkene flipping in **7b** is estimated to be k_{flip} = 290(80) s^{-1} (C_6D_5Cl, −38 °C) from the excess line broadening of the $H_{allylic}$ signal of **7b** at δ 2.4. More precise line width measurements are precluded by the proximity of more intense signals. Alkene flipping in **7b** is ca. 14 times faster than in **7a**.

Scheme 7. Possible C=C Double Bond Rotation Mechanism for Alkene Face Exchange

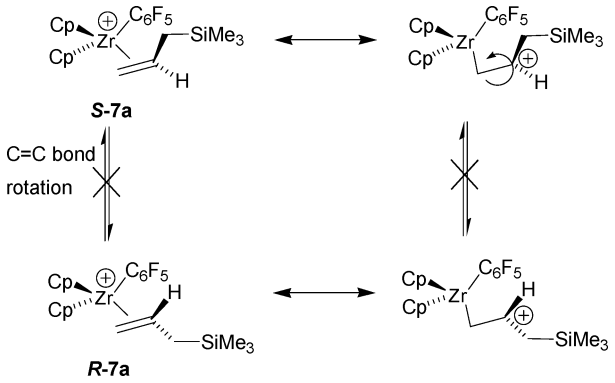

Mechanism of Alkene Flipping. Several mechanisms for alkene flipping in **7a**,**b** can be proposed, based on the framework of Gladysz.[33] Considered here are mechanisms involving double bond rotation, allyl-type intermediates, or C−H σ-complex intermediates.[34] Mechanisms which involve loss of alkene (eq 1 and Scheme 6) can be rejected since alkene flipping is significantly faster than alkene decomplexation.

Rotation around the ATMS C=C double bond would lead to enantioface exchange in **7a**,**b** (Scheme 7), and may be possible due to the polarized nature of this bond. This process has been established for $CpFe(CO)_2(\eta^2\text{-}H_2C{=}CHNR_2)^+$ alkene complexes.[35] This process exchanges the two Cp groups and the two $H_{allylic}$ hydrogens, and, significantly, also exchanges H_{trans} with H_{cis}. However, as noted above, the excess broadening of the H_{trans} and *p*-F signals are the same over a wide temperature range.[27] In addition, ^{1}H EXSY NMR spectra of **7a** do not exhibit cross-peaks between the H_{cis} and H_{trans} resonances. Therefore, H_{trans}/H_{cis} exchange does not occur, and double bond rotation is ruled out for **7a**,**b**.

Deprotonation of an allylic hydrogen or heterolytic $C_{allylic}$−Si bond cleavage of **7a**,**b** would lead to neutral η^1-allyl complexes (Scheme 8). Rotation around the "C_{term}−C_{int}" bond (i.e. the $ZrCH_2$−$CHCHSiMe_3$ or $ZrCH_2$−$CHCH_2$ bonds) of the allyl intermediates followed by reformation of the $C_{allylic}$−H or $C_{allylic}$−Si bonds would lead to net enantioface exchange in **7a**,**b**. However, these mechanisms also result in net C=C bond rotation and exchange of H_{trans} with H_{cis}, and thus can be rejected. In addition, a base would be required to deprotonate $H_{allylic}$. Bases are not present under the reaction conditions and in any case would likely displace ATMS from **7a**,**b**. Also, a transient $SiMe_3^+$ cation would likely react with other species in solution.

The NMR results for **7a**,**b** are, however, fully consistent with alkene enantioface exchange occurring via C−H σ-complex

(32) An Eyring analysis for alkene enantioface exchange was precluded by a narrow viable-temperature range (15 °C) and the small chemical shift difference of the two ^{1}H NMR Cp resonances of **7a**.

(33) Peng, T.-S.; Gladysz, J. A. *J. Am. Chem. Soc.* **1992**, *114*, 4174.

(34) (a) A reversible C_6F_5 insertion mechanism was also considered. However, while reversible C_6F_5 insertion would exchange the Cp rings (due to site epimerization in the insertion products), it does not exchange the allylic hydrogens. In addition, the insertion products would be more reactive towards insertion than **4a** itself, and ATMS polymerization would be observed, which is not the case. (b) Mechanisms considered by Gladysz[33] and involving, for example, oxidative addition or M−carbene formation, are not reasonably possible for **7a**,**b**.

(35) (a) Matchett, S. A.; Zhang, G.; Frattarelli, D. *Organometallics* **2004**, *23*, 5440. (b) Chang, T. C. T.; Foxman, B. M.; Rosenblum, M.; Stockman, C. *J. Am. Chem. Soc.* **1981**, *103*, 7361.

Scheme 8. Possible Allyl-Intermediate Mechanisms for Alkene Face Exchange

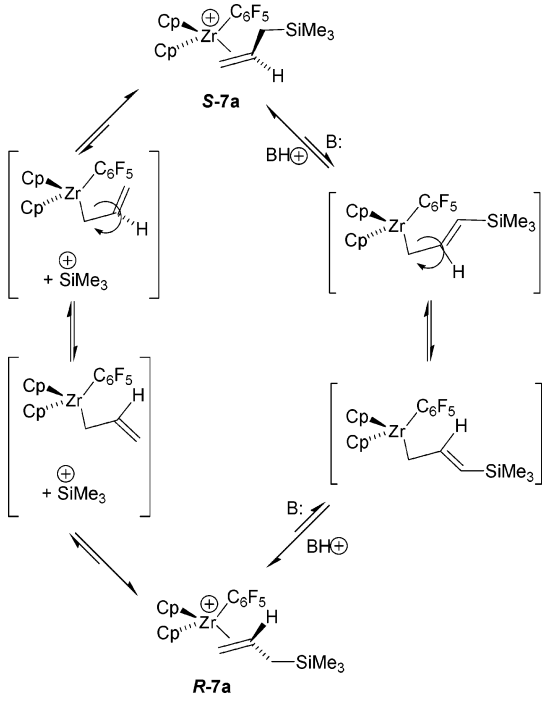

Scheme 9. Alkene σ-Complex Intermediate or Transition State Mechanism for Alkene Face Exchange

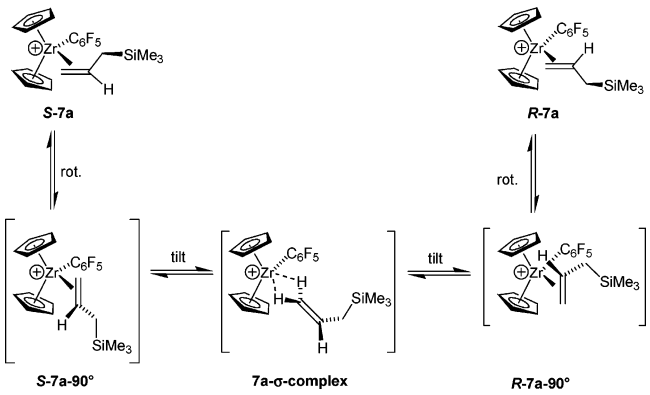

intermediates (Scheme 9). Steric crowding between the ATMS and Cp ligands during metal−(alkene centroid) rotation can be relieved by isomerization of the π-complex to a κ^2-$H_2C{=}CHR$ σ-complex intermediate or transition state, which can then relax to the π-complex by slippage of the $Cp_2Zr(C_6F_5)^+$ unit back to either enantioface.[36] The weaker π coordination for **7b** compared to that for **7a** explains the faster alkene flipping in **7b**.

The σ complex mechanism in Scheme 9 is similar to that proposed by Gladysz for Re^{I}.[33] Alkene flipping has also been proposed to occur by this mechanism in Zr^{IV}-catalyzed olefin polymerization.[30,37] For example, polymerization of isotopically labeled propylenes gives specifically labeled chain ends that have been explained in part by alkene flipping,[37a−c] and *trans*-1,3-enchainment in cyclopentene polymerization has been explained by this process.[37d]

Brintzinger proposed that alkene flipping in $Cp_2Zr(H)(H_2C{=}CMe_2)^+$ occurs via a κ^2-$H_2C{=}CMe_2$ C−H σ-complex, based on DFT studies.[30] The barrier for this process was calculated to be 8.1 kcal/mol, which is only slightly lower than the barriers found for alkene flipping in **7a**,**b**. The calculated barrier for alkene flipping of coordinated *cis*-2-butene via a κ^2-Me*HC*=*CH*Me σ-complex is much higher (19 kcal/mol).[30]

Neither the $SiMe_3$ group nor the C_6F_5 ligand is necessary per se for alkene flipping to occur. These groups simply strengthen the metal−alkene interaction and increase the alkene decomplexation barrier sufficiently to allow alkene flipping to be detectable and separable from the intermolecular exchange process in eq 1. Alkene flipping was not detected for **9** or other $Cp'_2Zr(O^tBu)(alkene)^+$ complexes at −89 °C in CD_2Cl_2, or for **9** at −38 °C in C_6D_5Cl. Alkene flipping is certainly possible in these cases, but would be masked by fast alkene decomplexation.

Intermolecular Alkyne Exchange. PTMS decomplexation from **8a** is much slower than ATMS decomplexation from **7a**, consistent with the greater binding strength of PTMS vs that of ATMS (Table 3). No significant NMR line broadening of the PTMS signals of **8a** is observed at −38 °C in C_6D_5Cl, implying that $k_{-1} \leq 3\ s^{-1}$. However, the ^1H EXSY spectrum of an **8a**/**4a**/PTMS equilibrium mixture (C_6D_5Cl, −38 °C, $\tau_m = 1.6$ s) contains exchange cross-peaks between the Cp resonances of **8a** and **4a** and between the free and coordinated alkyne CH_2 resonances. This result shows that **8a** exchanges with **4a** and free PTMS on the T_1 time scale, consistent with eq 1.

Reactivity of $Cp_2Zr(C_6F_5)(ATMS)^+$ and $Cp_2Zr(C_6F_5)(PTMS)^+$. When an equilibrium mixture of **4a**, **7a**, and free ATMS in C_6D_5Cl is warmed from −38 to +2 °C over 4 h, **7a** and free ATMS are consumed, and 6,6-dimethyl-4-((trimethylsilyl)methyl)-6-silahept-1-ene (**12**), a dimer of ATMS, is formed. Compound **12** results from a Lewis acid-mediated dimerization[38] of ATMS due to **4a**, or possibly trace Ph_3C^+.[39] NMR and GC/MS analysis of the organic products from a **4a**/**7a**/ATMS mixture maintained at 22 °C for 3 days shows the presence of dimers and trimers of ATMS. While the structures of these products were not determined, none contain C_6F_5 groups. The trimers likely form by a Lewis acid-mediated allylsilylation of **12**.[38] In addition, ca. 65% of **4a** remains after this time, but new Cp_2Zr species were not observed, and the fate of the consumed Zr is unknown. There is no evidence for ATMS insertion in **7a** by NMR or GC/MS. Bochmann reported that solutions of $[Cp_2Zr(C_6F_5)][(\mu\text{-Me})B(C_6F_5)_3]$ polymerize ethylene but noted that this behavior may be due to impurities.[11]

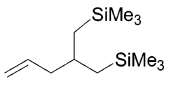

12

When an equilibrium mixture of **4a**, **8a**, and free PTMS in C_6D_5Cl is maintained at 22 °C for 14 h, 52% of **4a** is consumed, **8a** and free PTMS are fully consumed, and C_6F_5H is formed in 31% yield, as determined by NMR spectroscopy. These results suggest that protonolysis of the Zr−C_6F_5 bond of **8a** by PTMS

(36) Enantioface exchange in **7a**,**b** by dissociation of into **4a**,**b** and ATMS followed by recombination within a solvent cage, with slower diffusion of ATMS out of the cage, cannot be definitively excluded.
(37) (a) Sillars, D. R.; Landis, C. R. *J. Am. Chem. Soc.* **2003**, *125*, 9894. (b) Yoder, J. C.; Bercaw, J. E. *J. Am. Chem. Soc.* **2002**, *124*, 2548. (c) Leclerc, M. K.; Brintzinger, H. H. *J. Am. Chem. Soc.* **1996**, *118*, 9024. (d) Kelly, W. M.; Wang, S.; Collins, S. *Macromolecules* **1997**, *30*, 3151.
(38) Yeon, S. H.; Lee, B. W.; Yoo, B. R.; Suk, M.-Y.; Jung, I. N. *Organometallics* **1995**, *14*, 2361.
(39) Schade, C.; Mayr, H. *Makromol. Chem., Rapid Commun.* **1988**, *9*, 477.

occurs to yield C_6F_5H and the $Cp_2Zr(C{\equiv}CCH_2SiMe_3)^+$ cation, which can then catalytically oligomerize PTMS.[40] There is no evidence for PTMS insertion into the $Zr-C_6F_5$ bond of **8a**.

Reactivity of ATMS with Cp_2ZrMe^+. The successful observation of **7a**,**b** suggested that coordination of ATMS to other, more reactive d^0 Zr−carbyl cations may also be detectable by NMR spectroscopy. Therefore, the reaction of ATMS with Cp_2ZrMe^+ was probed. Addition of ATMS to a CD_2Cl_2 solution of $[Cp_2ZrMe][B(C_6F_5)_4]$ at −78 °C results in an immediate color change from yellow-orange to orange. NMR spectra of this mixture at −89 °C show that Cp_2ZrMe^+ and ATMS are completely consumed within the combined time periods of 1 min at −78 °C and 10 min at −89 °C. No resonances indicative of a d^0 metal−alkene complex and no NMR line broadening effects that can be ascribed to fast exchange between free and coordinated ATMS are observed. Instead, broad resonances for poly- or oligo(ATMS) are present, implying that ATMS insertion is fast even at low temperature.[41]

Conclusions

The combined use of strongly coordinating β-Si-substituted alkenes and alkynes, and the poorly nucleophilic C_6F_5 ligand enables the generation of stable Zr^{IV}−aryl−alkene and −alkyne complexes. Both tactics are necessary: non-β-Si substituted substrates such as 2-butyne do not coordinate to $[Cp_2Zr(C_6F_5)][B(C_6F_5)_4]$ (**4a**), and Cp_2ZrMe^+ rapidly oligomerizes or polymerizes ATMS even at −78 °C. ATMS and C_6D_5Cl compete in an equilibrium for coordination to $Cp_2Zr(C_6F_5)^+$. $[Cp_2Zr(C_6F_5)(H_2C{=}CHCH_2SiMe_3)][B(C_6F_5)_4]$ (**7a**) is more stable than $[Cp'_2Zr(C_6F_5)(H_2C{=}CHCH_2SiMe_3)][B(C_6F_5)_4]$ (**7b**), mainly due to Cp electronic effects.[17] Compounds **7a**,**b** exhibit divergent ^{13}C NMR chemical shifts for the alkene carbons (C_{int} shifts downfield; C_{term} shifts upfield) and a low-field ^1H NMR chemical shift for H_{int}. These data imply that the ATMS ligands in **7a**,**b** are significantly polarized and are bound in an unsymmetrical manner ($d(Zr-C_{int}) > d(Zr-C_{term})$) as observed for $(C_5R_5)_2Zr(alkoxide-alkene)^+$ species.[3] The similarity of the NMR data of **7a**,**b** to data for **9** and other Zr−alkoxide−alkene species shows that Zr−OR π-bonding does not contribute to the unsymmetrical alkene coordination observed in these systems.

Compounds **7a**,**b** undergo nondissociative alkene enantioface exchange, i.e., "alkene flipping," probably via σ-κ^2-$H_2C{=}CHCH_2SiMe_3$ intermediates or transition states. Similar processes have been proposed to occur during Zr-catalyzed alkene polymerization,[30,37] and may play a role in stereoselective α-olefin polymerization by chiral zirconocenes. The free energy barrier to alkene flipping in **7a**,**b** is similar to the barriers for initiation and propagation in 1-hexene polymerization by [*rac*-(EBI)ZrMe][$MeB(C_6F_5)_3$] (EBI = 1,2-(1-indenyl)$_2$ethane),[42] suggesting that its occurrence in polymerization is kinetically feasible.

(40) (a) Horton, A. D. *Chem. Commun.* **1992**, 185. (b) Akita, M.; Yasuda, H.; Nakamura, A. *Bull. Chem. Soc. Jpn.* **1984**, *57*, 480. (c) den Haan, K. H.; Wielstra, Y.; Teuben, J. H. *Organometallics* **1987**, *6*, 2053. (d) Heeres, H. J.; Teuben, J. H. *Organometallics* **1991**, *10*, 1980.

(41) Zirconocene catalysts polymerize ATMS by the same coordination/insertion mechanism as for other olefins, and exhibit the same metallocene-symmetry/polymer-tacticity relationships. (a) Resconi, L.; Piemontesi, F.; Franciscono, G.; Abis, L.; Fiorani, T. *J. Am. Chem. Soc.* **1992**, *114*, 1025. (b) Habaue, S.; Baraki, H.; Okamoto, Y. *Macromol. Chem. Phys.* **1998**, *199*, 2211. (c) Natta, G.; Mazzanti, G.; Longi, P.; Bernardini, F. *J. Polym. Sci.* **1958**, *31*, 181.

(42) Liu, Z.; Somsook, E.; White, C. B.; Rosaaen, K. A.; Landis, C. R. *J. Am. Chem. Soc.* **2001**, *123*, 11193.

Experimental Section

General Procedures. All reactions were performed using glovebox or Schlenk techniques under a purified N_2 atmosphere, or on a high vacuum line. N_2 was purified by passage through columns of activated molecular sieves and Q-5 oxygen scavenger. CD_2Cl_2 and C_6D_5Cl were distilled from P_2O_5. C_6D_6 was distilled from Na/benzophenone. Toluene was dried by passage through columns of activated alumina and BASF R3-11 oxygen-removal catalyst. $Cp_2Zr(C_6F_5)_2$ (**2a**),[10] $Cp_2Zr(C_6F_5)Me$ (**3a**),[11] $[HNMePh_2][B(C_6F_5)_4]$,[43] Cp_2ZrMe_2,[44] and Cp'_2ZrMe_2[45] were synthesized by literature methods. $Al(C_6F_5)_3{\cdot}1.2PhMe$ was synthesized by a literature method,[11] and the toluene content was determined by ^1H NMR spectroscopy with C_6Me_6 as an internal standard. **CAUTION: $Al(C_6F_5)_3{\cdot}PhMe$ is thermally and shock sensitive!** Other chemical were obtained from standard suppliers. $[Ph_3C][B(C_6F_5)_4]$ and $B(C_6F_5)_3$ were used as received. Allyltrimethylsilane and *tert*-butyl vinyl ether were dried over CaH_2. Bromobenzene, 2-butyne, and propargyltrimethylsilane were dried over 3 Å molecular sieves. Propyne was used as received. Elemental analyses were performed by Midwest Microlab (Indianapolis, IN).

NMR spectra were recorded on Bruker DRX 500 or 400 spectrometers in Teflon-valved NMR tubes at ambient probe temperature unless otherwise noted. ^1H and ^{13}C chemical shifts are reported relative to $SiMe_4$ and were referenced to the residual solvent signals. ^{19}F NMR spectra are reported relative to external $CFCl_3$ and were referenced either to external neat $CFCl_3$ or the *o*-F signal of internal C_6F_5H (δ −138.0, dd, J = 22, 9). ^{11}B NMR spectra are referenced to external $BF_3{\cdot}OEt_2$. NMR probe temperatures were calibrated by a MeOH thermometer.[46] Coupling constants are reported in hertz. Where $^{13}C\{$gated $^1H\}$ NMR spectra are reported, standard $^{13}C\{^1H\}$ NMR spectra were also recorded to assist in interpretation and assignment. For $H_2C{=}CHX$ substrates, H_{cis} is the H that is cis to H_{int}, and H_{trans} is the H that is trans to H_{int}.

NMR spectra of ionic compounds contain $B(C_6F_5)_4^-$ resonances at the free anion positions. ^{19}F NMR spectra were obtained for all compounds that contain this anion. NMR spectra of cationic compounds generated in situ by methide abstraction using Ph_3C^+ contain resonances for Ph_3CMe. The NMR data for $B(C_6F_5)_4^-$ and Ph_3CMe are given in the Supporting Information.

The ^{13}C NMR resonances of the C_6F_5 groups in the compounds described below were not detected due to low receptivity, overlap with $B(C_6F_5)_4^-$ resonances, or exchange line broadening.

$Cp'_2Zr(C_6F_5)Me$ (3b). A colorless solution of $Al(C_6F_5)_3{\cdot}1.2PhMe$ (0.1894 g, 0.297 mmol, 0.335 equiv) in toluene (20 mL) was added to a colorless solution of Cp'_2ZrMe_2 (0.2476 g, 0.886 mmol) in toluene (20 mL) by cannula over 5 min at 22 °C. The mixture turned yellow during the addition. The mixture was stirred for 15 min at 22 °C. The color changed to apricot after 10 min. The volatiles were removed under vacuum, and the residue was dried under vacuum for 2 d, yielding a pink powder. This material was sublimed (120 °C, 0.1 mTorr), yielding pure **3b** as a pale-yellow powder (0.192 g, 50%). ^1H NMR (C_6D_6): δ 5.74 (q, J = 2.4, 2H, Cp' CH), 5.55 (q, J = 2.5, 2H, Cp' CH), 5.52 (q, J = 2.5, 2H, Cp' CH), 5.26 (q, J = 2.4, 2H, Cp' CH), 1.75 (s, 6H, Cp'*Me*), 0.29 (t, J_{CF} = 4.0, 3H, ZrMe). $^{19}F\{^1H\}$ NMR (C_6D_6): δ −113.9 (br d, J = 24, 2F, *o*-F), −155.7 (t, J = 20, 1F, *p*-F), −161.4 (br m, 2F, *m*-F). $^{13}C\{^1H\}$ NMR (C_6D_6): δ 125.0 (ipso Cp'), 114.6 (Cp' CH), 113.7 (Cp' CH), 108.6 (Cp' CH), 106.9 (Cp' CH), 43.7 (t, J_{CF} = 7, ZrMe), 14.8 (Cp'*Me*). Anal. Calcd for $C_{19}H_{17}F_5Zr$: C, 52.88; H, 3.97. Found: C, 52.87; H, 4.04.

Generation of $[Cp_2Zr(C_6F_5)][B(C_6F_5)_4]$ (4a). To an NMR tube charged with $Cp_2Zr(C_6F_5)Me$ (**3a**, 16.4 mg, 0.0406 mmol) and $[Ph_3C][B(C_6F_5)_4]$ (37.7 mg, 0.0409 mmol) was added by vacuum transfer C_6D_5-

(43) Tjaden, E. B.; Swenson, D. J.; Jordan, R. F.; Petersen, J. L. *Organometallics* **1995**, *14*, 371.

(44) Samuel, E.; Rausch, M. D. *J. Am. Chem. Soc.* **1973**, *95*, 6263.

(45) Couturier, S.; Tainturier, G.; Gautheron, B. *J. Organomet. Chem.* **1980**, *195*, 291.

(46) Van Geet, A. L. *Anal. Chem.* **1970**, *42*, 679.

Cl at −196 °C. The tube was warmed to 22 °C and *vigorously* shaken to give an orange-yellow solution. The tube was allowed to sit at 22 °C for 2 d, during which time the solution turned yellow. NMR spectra showed that **4a** (97−99%), Ph_3CMe, and trace amounts (1−3%) of C_6F_5H and $[\{Cp_2Zr(C_6F_5)\}_2(\mu\text{-Cl})][B(C_6F_5)_4]$ (**6a**, see below) were present.[47] **Data for 4a:** ^1H NMR (C_6D_5Cl): δ 6.03 (s, 10H, Cp). ^1H NMR (C_6D_5Cl, −38 °C): δ 5.97 (s, 10H, Cp). ^{19}F NMR (C_6D_5Cl): δ −129.6 (br s, 2F, *o*-F), −150.1 (t, $J = 20$, 1F, *p*-F), −157.4 (br m, 2H, *m*-F). ^{19}F NMR (C_6D_5Cl, −38 °C): δ −118.2 (v br s, 1F, *o*-F), −140.0 (v br s, 1F, *o*-F), −150.4 (t, $J = 20$, 1F, *p*-F), −157.7 (br s, 2F, *m*-F). $^{13}C\{^1H\}$ NMR (C_6D_5Cl): δ 117.0 (Cp). $^{13}C\{^1H\}$ NMR (C_6D_5Cl, −38 °C): δ 117.0 (Cp).

Generation of $[Cp'_2Zr(C_6F_5)][B(C_6F_5)_4]$ (4b). To an NMR tube charged with **3b** (10.1 mg, 0.0234 mmol) and $[Ph_3C][B(C_6F_5)_4]$ (21.2 mg, 0.0230 mmol), was added by vacuum transfer C_6D_5Cl at −196 °C. The tube was warmed to 22 °C and shaken to give an orange-yellow solution. The tube was allowed to sit at 22 °C for 30 min, during which time the solution turned yellow. NMR spectra showed that **4b** (93%), Ph_3CMe, and small amounts (7−8% each) of C_6F_5H and an unknown impurity were present.[48] **Data for 4b:** ^1H NMR (C_6D_5Cl): δ 5.90 (br t, $J = 2$, 4H, Cp' CH), 5.80 (br t, $J = 2$, 4H, Cp' CH), 1.65 (s, 6H, Cp'*Me*). ^1H NMR (C_6D_5Cl, −38 °C): 5.84 (br s, 4H, Cp' CH), 5.73 (br s, 4H, Cp' CH), 1.59 (s, 6H, Cp'*Me*). ^{19}F NMR (C_6D_5Cl): δ −129.3 (v br s, 2F, *o*-F), −149.7 (t, $J = 19$, 1F, *p*-F), −157.1 (br s, 2F, *m*-F). ^{19}F NMR (C_6D_5Cl, −38 C): δ −116.7 (br s, 1F, *o*-F), −140.7 (br s, 1F, *o*-F-μ-Zr), −149.9 (t, $J = 20$, 1F, *p*-F), −155.9 (br s, 1F, *m*-F), −158.5 (br s, 1F, *m*-F). $^{13}C\{^1H\}$ NMR (C_6D_5Cl): δ 133.6 (ipso Cp'), 118.8 (Cp' CH), 114.2 (Cp' CH), 14.3 (Cp'*Me*). $^{13}C\{^1H\}$ NMR (C_6D_5Cl, −38 °C): δ 133.6 (ipso Cp'), 119 (v br, Cp' CH), 118 (v br, Cp' CH), 114.0 (br, Cp' CH), 14.5 (Cp'*Me*).

Generation of $[\{Cp'_2Zr(C_6F_5)\}_2(\mu\text{-Me})][B(C_6F_5)_4]$ (5b). To an NMR tube charged with **3b** (17.0 mg, 0.0394 mmol) and $[Ph_3C][B(C_6F_5)_4]$ (17.9 mg, 0.0194 mmol) was added by vacuum transfer C_6D_5Cl (0.60 mL) at −196 °C. The tube was warmed to 22 °C and shaken, giving a pale-yellow solution. NMR spectra at ambient probe temperature showed that **5b** (0.025 M), **3b** (0.014 M), **4b** (0.0048 M), and Ph_3CMe were present. The signals for the three Zr species were broad due to chemical exchange. Additional $[Ph_3C][B(C_6F_5)_4]$ (7.0 mg) was added. NMR spectra showed that the concentrations of **5b** (0.021 M), **3b** (0.0028 M), and **5b** (0.018 M) had changed. The signals for the Zr species again displayed significant NMR line broadening. At −38 °C, only **5b** (0.024 M) and **4b** (0.018 M) were present. **Data for 5b:** ^1H NMR (C_6D_5Cl): δ 6.00 (br s, 4H, Cp' CH), 5.96 (br s, 4H, Cp' CH), 5.90 (br s, 8H, Cp' CH), 1.81 (br s, 12H, Cp'*Me*), −0.24 (br s, 3H, μ-Me). ^1H NMR (C_6D_5Cl, −38 °C): δ 5.99 (t, 8H, Cp' CH), 5.91 (q, 4H, Cp' CH), 5.84 (br m, 4H, Cp' CH), 1.77 (s, 12H, Cp'*Me*), −0.27 (s, 3H, μ-Me). ^{19}F NMR (C_6D_5Cl): δ −116 (v br s, 4F, *o*-F), −151.4 (t, $J = 18$, 2F, *p*-F), −158.7 (br s, 4F, *m*-F). ^{19}F NMR (C_6D_5Cl, −38 °C): δ −112.6 (m, 2F, *o*-F), −120.6 (m, 2F, *o*-F), −151.6 (t, $J = 19$, 2F, *p*-F), −158.1 (br m, 2F, *m*-F), −159.4 (br m, 2F, *m*-F). $^{13}C\{^1H\}$ NMR (C_6D_5Cl): δ 130.5 (ipso Cp'), 118.2 (Cp' CH), 116.2 (Cp' CH), 112.7 (Cp' CH), 112.2 (Cp' CH), 14.8 (Cp'*Me*). $^{13}C\{^1H\}$ NMR (C_6D_5Cl, −38 °C): δ 130.4 (ipso Cp'), 117.6 (Cp' CH), 116.2 (Cp' CH), 112.4 (Cp' CH), 112.1 (Cp' CH), 32.2 (br m, μ-Me), 15.0 (Cp'*Me*).

Independent Generation of $[\{Cp_2Zr(C_6F_5)\}_2(\mu\text{-Cl})][B(C_6F_5)_4]$ (6a). A solution of $[Cp_2Zr(C_6F_5)][B(C_6F_5)_4]$ (**4a**, 0.028 mmol) in C_6D_5Cl was prepared in an NMR tube, and $[^nBu_3NCH_2Ph]Cl$ (3.1 mg, 0.0099 mmol) was added. The tube was sealed and shaken at 22 °C, resulting in an orange-yellow solution. NMR spectra revealed the presence of **6a** (72%) and unreacted **4a** (23%). **Data for 6a:** ^1H NMR (C_6D_5Cl): δ 6.20 (br s, 20H, Cp). ^1H NMR (C_6D_5Cl, −38 °C): δ 6.18 (s, 20H, Cp). ^{19}F NMR (C_6D_5Cl): δ −118.5 (br s, 4F, *o*-F), −151.6 (t, $J = 19$, 2F, *p*-F), −159.2 (br m, 4F, *m*-F). ^{19}F NMR (C_6D_5Cl, −38 °C): δ −114.6 (br s, 2F, *o*-F), −121.4 (br s, 2F, *o*-F), −151.7 (t, $J = 20$, 2F, *p*-F), −159.7 (v br s, 4F, *m*-F). $^{13}C\{^1H\}$ NMR (C_6D_5Cl): δ 116.6 (Cp). $^{13}C\{^1H\}$ NMR (C_6D_5Cl, −38 °C): δ 116.7 (Cp).

Generation of $[Cp_2Zr(C_6F_5)(H_2C{=}CHCH_2SiMe_3)][B(C_6F_5)_4]$ (7a). A solution of $[Cp_2Zr(C_6F_5)][B(C_6F_5)_4]$ (**4a**, 0.0268 mmol) in C_6D_5Cl (0.58 mL) in an NMR tube was cooled to −196 °C, and ATMS (0.13 mmol) was added by vacuum transfer. The tube was warmed to −40 °C and shaken, resulting in an orange-yellow solution. The tube was placed in an NMR probe that had been precooled to − 38 °C. NMR spectra showed the presence of **7a** (0.029 M), **4a** (0.018 M), and free ATMS (0.20 M). **Data for 7a:** ^1H NMR (C_6D_5Cl, −38 °C): δ 7.63 (m, 1H, C_{int}), 6.06 (br s, 5H, Cp), 6.00 (br s, 5H, Cp), 4.06 (d, $J =$ 16.5, 1H, H_{trans}), 3.84 (br t, $J = 8$, 1H, H_{cis}), 2.41 (br m, 1H, $H_{allylic}$), 2.07 (br m, 1H, $H_{allylic}$), 0.02 (s, 9H, $SiMe_3$). ^{19}F NMR (C_6D_5Cl, −38 °C): δ −151.2 (t, $J = 19$, 1F, *p*-F), −158.6 (br s, 2F, *m*-F). The *o*-F resonances were not detected due to line broadening. $^{13}C\{$gated $^1H\}$ NMR (C_6D_5Cl, −38 °C): δ 186.5 (dm, $^1J_{CH} = 161$, C_{int}), 116.4 (br d, $^1J_{CH} = 184$, Cp), 116.2 (br d, $^1J_{CH} = 184$, Cp), 97.7 (tm, $^1J_{CH} = 150$, C_{term}), 37.0 (t, $^1J_{CH} = 129$, $C_{allylic}$), −2.0 (q, $^1J_{CH} = 120$, $SiMe_3$). The C_{int} and C_{term} resonances show unresolved coupling to the C_6F_5 ligand.

Generation of $[Cp_2Zr(C_6F_5)(THF)][B(C_6F_5)_4]$ (10a). A solution of $[Cp_2Zr(C_6F_5)][B(C_6F_5)_4]$ (**4a**, 0.0235 mmol) in C_6D_5Cl in an NMR tube was cooled to −196 °C, and THF (0.216 mmol) was added by vacuum transfer. The tube was warmed to 22 °C and shaken, resulting in an orange-yellow solution. The volatiles were removed under vacuum at 22 °C, and C_6D_5Cl was added at −196 °C. The tube was warmed to 22 °C and shaken, giving an orange-yellow solution. NMR spectra revealed the presence of **10a** (93%) and Ph_3CMe. ^1H NMR (C_6D_5Cl): δ 6.08 (s, 10H, Cp), 3.67 (br m, 4H, THF), 1.57 (br m, 4H, THF). ^{19}F NMR (C_6D_5Cl): δ −119.7 (v br s, 2F, *o*-F), −151.1 (t, $J = 20$, 1F, *p*-F), −158.5 (m, 2F, *m*-F). $^{13}C\{^1H\}$ NMR (C_6D_5Cl): δ 116.4 (Cp), 81.8 (THF), 25.7 (THF).

Generation of $[Cp'_2Zr(C_6F_5)(H_2C{=}CHCH_2SiMe_3)][B(C_6F_5)_4]$ (7b). A solution of **4b** (0.0230 mmol) in C_6D_5Cl (0.58 mL) in an NMR tube was cooled to −196 °C, and ATMS (0.122 mmol) was added by vacuum transfer. The tube was warmed to −40 °C and shaken to give a yellow solution. The tube was placed in an NMR probe that had been precooled to −38 °C. NMR spectra showed that **7b** (0.015 M), **4b** (0.025 M), and free ATMS (0.27 M) were present. **Data for 7b:** ^1H NMR (C_6D_5Cl, −38 °C): δ 7.64 (m, 1H, H_{int}), 4.13 (d, $J = 16.0$, 1H, H_{trans}), 4.00 (br t, $J_{apparent} = 6$, 1H, H_{cis}), 2.4 (v br s, 1H, $H_{allylic}$), 2.1 (v br s, 1H, $H_{allylic}$, partially obscured), 1.67 (s, 6H, Cp'*Me*). The $SiMe_3$ and Cp' CH resonances are obscured by resonances of free ATMS. ^{19}F NMR (C_6D_5Cl, −38 °C): δ −113.3 (br s, 1F, *o*-F), −125.6 (br s, 1F, *o*-F), −150.8 (t, $J = 20$, 1F, *p*-F), −157.8 (br s, 1F, *m*-F), −158.7 (br s, 1F, *m*-F). $^{13}C\{^1H\}$ NMR (C_6D_5Cl, −38 °C): δ 184.9 (C_{int}), 97.9 (C_{term}), 36.7 ($C_{allylic}$), 14.8 (Cp'*Me*), −0.2 ($SiMe_3$). The Cp' ipso and CH resonances are broadened into the baseline due to exchange.

Generation of $[Cp_2Zr(C_6F_5)(HC{\equiv}CCH_2SiMe_3)][B(C_6F_5)_4]$ (8a). A solution of $[Cp_2Zr(C_6F_5)][B(C_6F_5)_4]$ (**4a**, 0.0233 mmol) in C_6D_5Cl (0.53 mL) in an NMR tube was cooled to −196 °C, and PTMS (0.027 mmol) was added by vacuum transfer. The tube was warmed to −40 °C and shaken, resulting in a maroon solution. The tube was then placed in an NMR probe that had been precooled to −38 °C. NMR spectra revealed the presence of **8a** (0.040 M), **4a** (0.0044 M), and free PTMS (0.011 M). **Data for 8a:** ^1H NMR (C_6D_5Cl, −38 °C): δ 6.04 (s, 10H, Cp), 4.44 (br s, 1H, ≡CH), 2.14 (br s, 2H, CH_2), 0.11 (s, 9H, $SiMe_3$). ^{19}F NMR (C_6D_5Cl, −38 °C): δ −114.6 (br s, 1F, *o*-F), −121.0 (br s, 1F, *o*-F), −151.5 (t, $J = 20$, 1F, *p*-F), −159.0 (br s, 2F, *m*-F). ^{13}C-{gated ^1H} NMR (C_6D_5Cl, −38 °C): δ 145.2 (d, $^2J_{C\equiv C_H} = 34$, C_{int}),

(47) Trace amounts (1−3%) of **6a** were observed in some samples of **4a**. Compound **6a** is formed at the beginning of the reaction and does not grow in at longer reaction times. **6a** is probably formed by the reaction of **4a** with alkyl chloride impurities in the solvent or trityl salt, or from Zr−Cl impurities in **3a**.

(48) The unknown impurity is probably $\{Cp'_2Zr(C_6F_5)\}_2(\mu\text{-Cl})^+$, analogous to **6a**.

116.1 (d, $^1J_{CH}$ = 178, Cp), 78.4 (dt, $^1J_{CH}$ = 232, $^4J_{CF}$ = 8, C_{term}), 16.8 (t, $^1J_{CH}$ = 135, CH_2), −1.9 (q, $^1J_{CH}$ = 121, $SiMe_3$).

Reaction of [Cp_2ZrMe][$B(C_6F_5)_4$] with Allyltrimethylsilane. To an NMR tube charged with Cp_2ZrMe_2 (6.0 mg, 0.0239 mmol) and [Ph_3C][$B(C_6F_5)_4$] (21.4 mg, 0.0232 mmol, 0.972 equiv) was added by vacuum transfer C_6D_5Cl at −196 °C. The tube was warmed to 22 °C and shaken to give an orange-yellow solution. After 4 h, a ^1H NMR spectrum was taken, which revealed the presence of [Cp_2ZrMe]-[$B(C_6F_5)_4$] and Ph_3CMe in a 1:1 ratio. The volatiles were removed under vacuum at 22 °C to give a dark oil, and CD_2Cl_2 was added by vacuum transfer at −78 °C. The tube was shaken and stored at this temperature, giving a yellow-orange solution. ATMS (0.118 mmol) was added by vacuum transfer at −196 °C. The tube was warmed to −78 °C and shaken, giving an orange solution. The tube was maintained at −78 °C for 1 min and then NMR spectra were recorded at −89 °C. The NMR spectra revealed that the Cp_2ZrMe^+ and ATMS were completely consumed and that resonances for $Cp_2Zr(Me)(ATMS)^+$ were absent. Instead, the ^1H NMR spectrum contained broad signals for oligo- or poly-ATMS at δ 1.7−0.5 and δ −0.07 ppm.[41] Numerous unidentified Cp resonances were observed by ^1H and ^{13}C NMR spectroscopy.

Determination of Thermodynamic Parameters and Exchange Rates. (A) General Variable-Temperature NMR Procedure. NMR samples were prepared as described above. The NMR tube was stored at −40 °C, and placed in a precooled NMR probe. The probe was maintained at a given temperature for 20−30 min to allow the sample to reach thermal equilibrium, and then NMR experiments were conducted. The temperature was raised 5 or 10 °C and the procedure repeated until the desired temperature range had been studied.

(B) Equilibrium Constant Measurements. The equilibrium constant for the reaction:

$$\mathbf{4a} + H_2C{=}CHCH_2SiMe_3 \rightleftarrows \mathbf{7a}$$

was defined to be $K_{eq} = [\mathbf{7a}][\mathbf{4a}]^{-1}[ATMS]^{-1}$. The concentrations of **7a**, **4a**, and free ATMS at equilibrium were determined by ^1H and ^{19}F NMR. This equilibrium constant was determined to be K_{eq} = 8.2(1.4) M^{-1} (C_6D_5Cl, −38 °C) from 8 measurements over the concentration ranges of $[\mathbf{4a}]_{initial}$ = 0.023−0.064 M and $[ATMS]_{initial}$ = 0.095−0.23 M. This K_{eq} was measured over the temperature range −38 to +2 °C, in 5 °C intervals.

The equilibrium constant for the reaction:

$$\mathbf{4b} + H_2C{=}CHCH_2SiMe_3 \rightleftarrows \mathbf{7b}$$

was defined to be $K_{eq} = [\mathbf{7b}][\mathbf{4b}]^{-1}[ATMS]^{-1}$ and found in a manner similar to that for **7a**. This equilibrium constant was determined to be K_{eq} = 2.4(2) M^{-1} (C_6D_5Cl, −38 °C) from three measurements over the concentration ranges of $[\mathbf{4b}]_{initial}$ = 0.029−0.040 M and $[ATMS]_{initial}$ = 0.015−0.29 M.

The equilibrium constant for the reaction:

$$\mathbf{4a} + HC{\equiv}CCH_2SiMe_3 \rightleftarrows \mathbf{8a}$$

was defined to be $K_{eq} = [\mathbf{8a}][\mathbf{4a}]^{-1}[PTMS]^{-1}$. The concentrations of **8a**, **4a**, and free PTMS at equilibrium were determined by ^1H NMR. The equilibrium constant was determined to be K_{eq} = 910(60) M^{-1} (C_6D_5Cl, −38 °C) by four measurements over concentrations ranges of $[\mathbf{4a}]_{initial}$ = 0.044−0.054 M and $[PTMS]_{initial}$ = 0.050−0.067 M.

Thermodynamic parameters ($\Delta H°$ and $\Delta S°$) for the reaction:

$$\mathbf{4a} + H_2C{=}CHCH_2SiMe_3 \rightleftarrows \mathbf{7a}$$

where $K_{eq} = [\mathbf{7a}][\mathbf{4a}]^{-1}[ATMS]^{-1}$ were determined from van't Hoff plots for two variable-temperature NMR runs using Minitab[49] to determine the thermodynamic parameters and their standard deviations. The reported values are the averages of the results of these two experiments.

(C) Exchange Rate Measurements by NMR Line Broadening. Variable-temperature ^1H and ^{19}F NMR spectroscopies were used to measure the kinetics of the dynamic processes of **7a**. The first-order rate constant for ATMS decomplexation from **7a** (k_{-1}) was determined by $k_{-1} = \pi\Delta\omega$, where $\Delta\omega$ is the excess line width due to exchange of the H_{trans} or *p*-F signals of **7a** and is defined by $\Delta\omega = \omega - \omega_0$, where ω is the actual line width of the H_{trans} or *p*-F resonances of **7a** and ω_0 is the line width of the Ph_3CMe or the *p*-F signal of **6a**. All line widths were found by simulation using gNMR.[50] The coupling constants between H_{trans}/H_{int} and *p*-F/*m*-F for **7a**, and between *p*-F/*m*-F of **6a** were found by simulation at all temperatures where these coupling are resolvable, but were extrapolated at other temperatures. The coupling between H_{trans}/H_{cis} was set to −5.1 Hz, that between $H_{trans}/H_{allylic}$ (δ 2.41) was set to −2.4 Hz, and that between $H_{trans}/H_{allylic}$ (δ 2.07) was set to −1.8 Hz. These values were found by simulation at −38 °C and kept constant with temperature. Eyring plots were used to determine activation parameters ($\Delta H_{-1}^{\ddagger}$and $\Delta S_{-1}^{\ddagger}$) for ATMS decomplexation from **7a** using both ^1H and ^{19}F NMR data.[49] Reported values are the weighted averages between two runs each of ^1H and ^{19}F NMR data (total of four plots).

(D) EXSY Spectroscopy. Two-dimensional ^1H EXSY NMR spectra of equilibrium mixtures of **7a**, **4a**, and free ATMS were obtained at −38 °C using the Bruker pulse program *noesytp*, with the pulse sequence d_1 − 90° − d_0 − 90° − τ_m − 90° − acquire. The spectral width consisted of the $H_{allylic}$ region (δ 2.85−1.08 ppm). The relaxation delay d_1 was set at 6.0 s, which was 4 times the longest T_1 of the signals in this region (determined by an inversion−recovery experiment). The mixing time τ_m was set to 50 ms, the acquisition time was set to 1.1 s, and the 90° pulse width was set to 10.3 μs. The initial d_0 value was 3 μs. The pulse sequence was repeated for 68 values of d_0, and the F_1 dimension was zero-filled to 2048 points. The F_2 dimension had 2048 points. The number of scans per experiment was 16. The baseline was automatically corrected in both dimensions, but the spectrum was not symmetrized about the diagonal.

Integrals of cross-peaks were symmetrical about the diagonal to within 10%. Due to overlap of the diagonal signal of the coordinated $H_{allylic}$ signal at δ 2.07 with that for Ph_3CMe (δ 2.01), the integral of this $H_{allylic}$ diagonal signal was assumed to be equal to the integral of the diagonal signal of the coordinated $H_{allylic}$ signal at δ 2.41. This assumption does not affect the integrals of any cross-peaks.

The EXSY data were analyzed using the procedure described by Perrin and Dwyer.[28] Rate constants were found from the rate constant/relaxation matrix **R**:

$$-\mathbf{R} = \begin{matrix} R_a & k_{b,a} & k_{f,a} \\ k_{a,b} & R_b & k_{f,b} \\ k_{a,f} & k_{b,f} & R_f \end{matrix}$$

where $k_{m,n}$ is the site-to-site rate constant for exchange from site m to site n, and R_n relates to both kinetic and relaxation data and is not considered here. Site a is the proton at the $H_{allylic}$ signal of **7a** at δ 2.41, site b is the proton at the $H_{allylic}$ signal of **7a** at δ 2.07, and site f are the protons at the free $H_{allylic}$ signal. Matrix **R** is related to EXSY integration data by $\mathbf{R} = -(1/\tau_m)\ln(\mathbf{A})$ (solved with MATLAB),[51] where **A** is the normalized spectral intensity matrix as follows:

$$\mathbf{A} = \begin{matrix} I_{aa}/p_a & I_{ab}/p_b & I_{af}/p_f \\ I_{ba}/p_a & I_{bb}/p_b & I_{bf}/p_f \\ I_{fa}/p_a & I_{fb}/p_b & I_{ff}/p_f \end{matrix}$$

(49) *Minitab*, v. 11.2; Minitab Inc.: State College, PA, 1996.

(50) *gNMR*, v. 4.1.2; Adept Scientific: Letchworth, UK, 2000.

(51) *MATLAB*, v. 5.0.0.4073; The Math Works, Inc.: Natick, MA, 1996.

where I_{xy} is the integral of the peak between site x and site y is listed schematically:

af	bf	ff
ab	bb	fb
aa	ba	fa

and corresponding to the EXSY spectrum in Figure 8, p_a is the population fraction occupying the coordinated $H_{allylic}$ resonance at δ 2.41, p_b is the population fraction occupying the coordinated $H_{allylic}$ signal at δ 2.07, and p_f is the population fraction occupying the free $H_{allylic}$ position. These population fractions are related to mole fractions of free ATMS (x_{free}) and **7a**-coordinated ATMS (x_{coord}) such that $p_f = x_{free}$ and $p_a = p_b = 0.5 \cdot x_{coord}$.

The site-to-site rate constants in **R** are related to rate constants for chemical exchange processes as follows: for alkene flipping between enantiofaces of **7a**, $k_{flip} = k_{a,b} = k_{b,a}$; for alkene decomplexation from **7a** to give free alkene and **4a**, $k_{dissoc} = k_{a,f} = k_{b,f}$; and for alkene complexation to **4a** to give **7a**, $k_{assoc,obs} = k_{assoc}[\mathbf{4a}] = 2 \cdot k_{f,a} = 2 \cdot k_{f,b}$. An EXSY spectrum containing the $H_{allylic}$, H_{cis}, and H_{trans} regions did not contain cross-peaks between coordinated H_{cis} and H_{trans}, nor between either of these signals to the coordinated $H_{allylic}$ signals.

Reported values for k_{dissoc} and k_{flip} are the averages from three EXSY spectra with mixing times of 20, 25, and 50 ms.

Acknowledgment. We thank the NSF (CHE-0212210) for financial support and the University of Chicago for a William Rainey Harper fellowship (E.J.S.).

Supporting Information Available: Additional experimental details, data for free substrates (pdf). This material is available free of charge via the Internet at http://pubs.acs.org.

JA057524P